Geology of Lonar Crater, India

Adam C. Maloof[1], Sarah T. Stewart[2], Benjamin P. Weiss[3], Samuel A. Soule[4], Nicholas L. Swanson-Hysell[1], Karin L. Louzada[2], Ian Garrick-Bethell[3], and Pascale M. Poussart[1]

[1]*Department of Geosciences, Princeton University, Guyot Hall, Washington Road, Princeton, New Jersey 08544, USA*

[2]*Department of Earth and Planetary Sciences, 20 Oxford Street, Cambridge, Massachusetts 02138, USA*

[3]*Department of Earth, Atmospheric, and Planetary Sciences, Massachusetts Institute of Technology, 77 Massachusetts Avenue, Cambridge, Massachusetts 02139, USA*

[4]*Woods Hole Oceanographic Institution, Geology and Geophysics, Woods Hole, Massachusetts 02543, USA*

ABSTRACT

Lonar Crater, India, is one of the youngest and best preserved impact structures on Earth. The 1.88-km-diameter simple crater formed entirely within the Deccan traps, making it a useful analogue for small craters on the basaltic surfaces of the other terrestrial planets and the Moon. In this study, we present a meter-scale–resolution digital elevation model, geological map of Lonar Crater and the surrounding area, and radiocarbon ages for histosols beneath the distal ejecta. Impact-related deformation of the target rock consists of upturned basalt flows in the upper crater walls and recumbent folding around rim concentric, subhorizontal, noncylindrical fold axes at the crater rim. The rim-fold hinge is preserved around 10%–15% of the crater. Although tearing in the rim-fold is inferred from field and paleomagnetic observations, no tear faults are identified, indicating that large displacements in the crater walls are not characteristic of small craters in basalt. One significant normal fault structure is observed in the crater wall that offsets slightly older layer-parallel slip faults. There is little fluvial erosion of the continuous ejecta blanket. Portions of the ejecta blanket are overlain by aerodynamically and rotationally sculpted glassy impact spherules, in particular in the eastern and western rim, as well as in the depression north of the crater known as Little Lonar. The emplacement of the continuous ejecta blanket can be likened to a radial ground-hugging debris flow, based on the preserved thickness distribution of the ejecta, the efficient exchange of clasts between the ejecta flow and the underlying histosol, and the lack of sorting and stratification in the bulk of the ejecta. The ejecta profile is thickened at the distal edge and similar to fluidized ejecta structures observed on Mars.

INTRODUCTION

Motivation

Impact cratering is a dominant surface modification process in the solar system, yet aspects of cratering mechanics remain poorly understood. Information about high strain-rate rock deformation and ejecta emplacement processes are recorded in the geology of impact structures. However, due to the high erosion rates on Earth, few craters have retained a complete record of the cratering process. Lonar Crater, India, is a young, well-preserved simple crater formed in the Deccan trap basalts, making it a rare analog for impact structures observed on the basaltic surfaces of other terrestrial planets and the Moon. The present study focuses on geologic mapping of Lonar Crater (Fig. 1), including the structural deformation around the rim and the physical properties of the ejecta blanket.

When a bolide impacts a planetary surface at hypervelocities, a shock wave propagates both down into the surface and up into the projectile, compressing both materials and slowing the projectile. A rarefaction wave from the rear of the projectile and the surrounding free surface overtakes the shock wave leading to a decaying hemispherical shock pulse. The decaying shock pulse generates an excavation flow field that moves material first downward, then up and outward, creating a hemispherical transient crater. The motion is accommodated by brecciation and deep fracturing in the target rocks and folding in the crater rim. In small (strength-dominated) craters, the excavation flow is impeded by the strength of the crater wall rock, and the transient cavity is widened and shallowed by slumping of the crater walls in the end stage of crater formation. Around large (gravity-dominated) craters, the shock deformation significantly weakens the rock mass, and the fluid-like collapse of the transient crater leads to significant widening and shallowing of the cavity and formation of central peak structures (Melosh, 1989; Melosh and Ivanov, 1999; Kenkmann, 2002).

The details of how rocks respond to the high stresses and strain-rates associated with impact cratering are still poorly understood (Herrick and Pierazzo, 2003). Laboratory-based studies have provided useful insights into the principal styles of fracturing beneath and around small (several-cm–scale) crater cavities (e.g., Polanskey and Ahrens, 1990; Ai and Ahrens, 2006), and seismic studies have estimated the depths of fracture zones (summarized in Ahrens et al., 2002). Three sets of fractures (conical, radial, and concentric) have been observed around strength-dominated craters in the laboratory and in the field. Structural deformation around simple impact craters is characterized by (1) brecciation (of ejected and displaced materials), (2) conical and radial fractures, (3) folding and tearing in the crater rim, (4) uplifted strata, and (5) listric faulting and slumping of the crater wall (e.g., Shoemaker, 1960; Brandt and Reimold, 1995; Kumar, 2005; Kumar and Kring, 2008). However, target lithologies and preexisting structural features influence the generation and activation of fractures during impact cratering (Kumar and Kring, 2008), which complicates the generalization of impact-induced deformation processes from the limited terrestrial data. More detailed geologic studies of terrestrial craters are needed to improve our understanding of cratering mechanics.

Much of our knowledge of impact ejection processes is derived from laboratory experiments and explosion craters (e.g., Roddy et al., 1977) and observations of lunar craters (e.g., Pike, 1976). The principal aspects of the formation of continuous ejecta structures are captured

†E-mail: sstewart@eps.harvard.edu

GSA Bulletin; January/February 2010; v. 122; no. 1/2; p. 109–126; doi: 10.1130/B26474.1; 12 figures; Data Repository item 2009131.

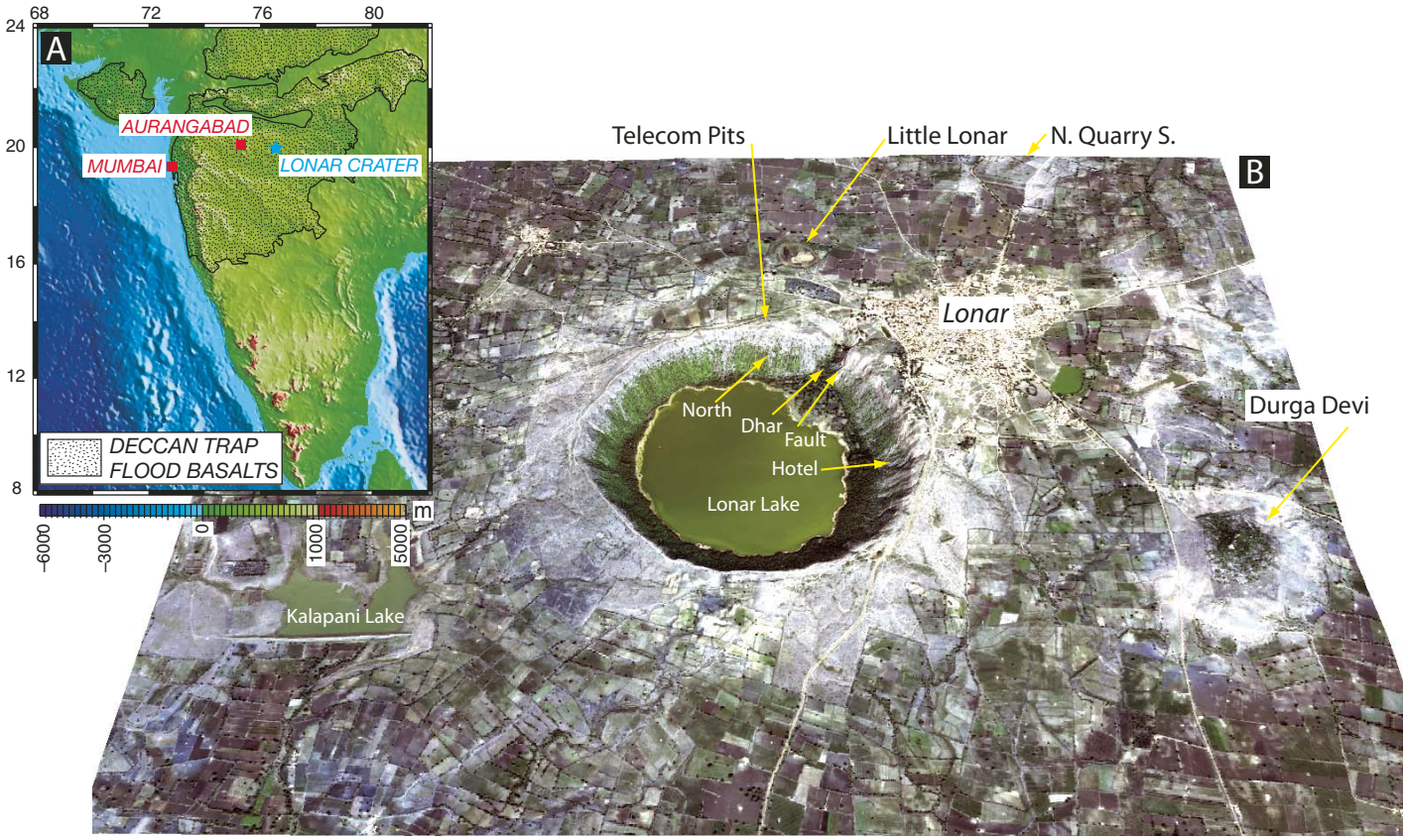

Figure 1. (A) EToPo2 (http://www.ngdc.noaa.gov/mgg/fliers/01mgg04.html) topography of India (color scale is in meters, coordinates in latitude and longitude), showing the extent of the Deccan Plateau (Deshmukh, 1988; Bondre et al., 2004) and the location of Lonar Crater; (B) Four-band, pan-sharpened, true-color Quickbird satellite image of Lonar Crater, draped on the digital elevation model of Figure 2. The locations of measured stratigraphic sections from Figure 3 are marked with yellow arrows. The crater rim diameter is 1.88 km.

by the ballistic erosion and sedimentation model (Oberbeck, 1975). In this model, an inclined curtain of ballistic ejecta impacts the surrounding terrain with increasing velocity from the crater rim outward. The thickness of the ballistic ejecta decreases with distance by about a –3 power law (McGetchin et al., 1973). Around small craters, the final ejecta blanket closely resembles the ballistic ejecta distribution. However, around larger craters, the ballistic ejecta impact with sufficient velocity to generate secondary craters that excavate the surrounding surface materials. The surface materials are mixed with the primary ejecta with enough outward momentum to generate a radial ground-hugging debris flow (of unpredicted travel distance). Hence, the final continuous deposits around large craters are composed of an increasing volume fraction of secondary materials with radial distance and a final thickness profile that is shallower than the ballistic ejecta profile (Oberbeck, 1975; Morrison and Oberbeck, 1978).

The best studied ejecta blankets around terrestrial craters reveal many aspects of ejecta dynamics that are still poorly understood. At the 1.2-km-diameter Barringer Crater (a.k.a. Coon Butte and Meteor crater), Arizona, the continuous ejecta blanket contains distal lobes (Grant and Schultz, 1993) suggesting that a ground-hugging flow modified an original power-law profile around a small simple crater. The ejecta blankets around the larger Ries (24 km) and Chicxulub (~170 km) impact structures record even larger ground-hugging flows. At Ries, the continuous ejecta deposit is characterized by a large volume fraction of secondary materials and ground-hugging debris surge (Hörz et al., 1983) in agreement with the ballistic sedimentation model. The extent of the debris surge is surprising, however, with clasts found as far as 10 km from their original location. At Ries, the large runout of ejecta flows has been attributed to decoupling of near-surface target material followed by dragging of the ejecta curtain along the surface (Kenkmann and Ivanov, 2006). At Chicxulub, the outward flow was likely accommodated by subsurface volatiles and the presence of basal glide planes (Kenkmann and Schonian, 2006). In addition, distinct ejecta layers (e.g., a ballistic layer overlain by a suevitic layer) have been identified at Ries (Osinski et al., 2004) and Chicxulub (Wittmann et al., 2007).

The record of ejecta processes is even more diverse on Mars. Martian ejecta morphologies have been described as layered or fluidized (Barlow et al., 2000; Barlow, 2005). Fluidized ejecta are found around all fresh, and many older, craters larger than a few km on Mars (Barlow, 2005). They are characterized by lobate profiles distinct from lunar power-law ejecta thickness profiles, longer runout distances than lunar craters, and sinuous and continuous terminal ramparts (Carr et al., 1977; Mouginis-Mark, 1978; Barlow and Bradley, 1990). These observations suggest that similar processes may affect ejecta blanket emplacement on Earth and Mars, which are distinct from the ballistic sedimentation model for the Moon and Mercury. Suggested mechanisms include the presence of an atmosphere (Schultz, 1992; Barnouin-Jha and Schultz, 1998, 1999) and/or the presence of subsurface volatiles such as liquid water or ice

(Carr et al., 1977; Barlow and Bradley, 1990; Stewart et al., 2004). On Earth, the high concentration of volatiles in sedimentary lithologies may also contribute to fluidization of the ejecta (Kieffer and Simonds, 1980).

Detailed observations of structural deformation and ejecta emplacement around simple craters are a means to improve our understanding of the primary dynamic deformation processes and may be used to refine cratering simulations. Although sketch maps of variable quality (LaTouche, 1912; Nayak, 1972; Fredriksson et al., 1973a; Ghosh, 2003) have been published, no digital elevation model (DEM) or detailed geologic map exists for Lonar Crater. In this study, we present a DEM, a geologic map, stratigraphic sections, and cross sections of Lonar Crater. We describe observations relevant to crater formation, deformation, and ejecta emplacement processes.

Background

Lonar Crater is an ~135-m-deep, ~1.88-km-diameter, near-circular depression in the Deccan Plateau (Fig. 1A and GSA Data Repository Fig. DR1[1]) of the Buldhana District, Maharashtra State, India. The rim rises 30 m, on average, above the surrounding plains. In the crater, there is a saline lake (LaTouche, 1912; Jhingran and Rao, 1958; Nandy and Deo, 1961), with a uniform depth of less than 6 m (Fig. 2). The crater cavity is filled with >225 m of breccia overlain by 30–100 m of unconsolidated sediment (Nandy and Deo, 1961; Fredriksson et al., 1973a; Fudali et al., 1980; Grieve et al., 1989). The main feeder stream to the lake enters the crater at the head of Dhar Canyon in the northeast (Fig. 1B). A temple is located at this site, and even in the dry winter months, the stream supplies Lonar town with potable water (Fig. DR2 [see footnote 1]). The outflow from Dhar Canyon has built a delta into Lonar Lake that currently is used for banana farming. A second perennial source of water emerges as a spring ~65 m below the main dhara (stream). The temple Ram-Gaya on the east side of the crater floor also hosts another small perennial spring. Lonar Lake has no stream outlet, and during dry years, a thick salt crust forms on the lake bed.

The geologic origin of Lonar Crater, a unique structure in an otherwise featureless Deccan Plateau (Malcolmson, 1840; Cotton, 1944), has been debated since at least Orlebar (1839). Most early visitors suggested a volcanic origin for the crater, emphasizing its location within a thick pile of basaltic volcanic rocks (Orlebar, 1839; Blanford, 1870; LaTouche, 1912), and argued that the Deccan basalts themselves erupted from Lonar Crater (Nandy and Deo, 1961). Others considered the crater to be cryptovolcanic in origin (Blanford, 1870; LaTouche, 1912; Subrahmanyam, 1985). These authors were led to a cryptovolcanic, or steam explosion, hypothesis because they realized that the thin sediment fill in the lake, the immature level of river incision, and slope diffusion of the crater wall, required a much younger age for the crater than the obvious antiquity of the Deccan basalt landscape. As recently as 1987, some authors have supported the cryptovolcanic hypothesis (Crawford, 1983; Subrahmanyam, 1985; Mishra, 1987).

In his discussion of Barringer Crater, Gilbert (1896) highlighted a few observations that made a bolide impact origin appealing (despite concluding that both Lonar and Barringer craters were of volcanic origin): (1) the crater is not composed of volcanic rock, and (2) there is an abundance of iron meteorite fragments strewn around the crater rim and adjacent plains. In contrast, as the early visitors noted, Lonar Crater is contained entirely within basaltic volcanic rocks, and no meteorite fragments have been found.

Eventually, the antiquity of the Deccan basalts compared to the physiographically very young crater and widely available information about sites like Barringer Crater led Beals et al. (1960) and Lafond and Dietz (1964) to propose an impact origin for Lonar. Soon thereafter, direct evidence of shocked materials such as maskelynite and impact glass were found at Lonar, and an impact origin for the crater became the leading hypothesis (Nayak, 1972; Fredriksson et al., 1973a; Fudali et al., 1980; Nayak, 1993; Sengupta et al., 1997; Ghosh, 2003; Storzer and Koeberl, 2004).

The mineralogy of the Deccan trap tholeiitic flood basalts is predominantly plagioclase (labradorite) and pyroxene (augite and pigeonite). The absence of quartz means that it is difficult to classify the shock level in these basalts, particularly at low to moderate shock levels (i.e., ~2–20 GPa), where shock-produced glasses are absent or rare. Early pioneering studies of the shock petrography of the Lonar Crater basalts were conducted by Schaal (1975) and Kieffer et al. (1976). These workers noted that the main shock effects are the conversion of plagioclase to diaplectic glass (maskelynite; Nayak, 1993) and vesiculated feldspar glass, and undulatory extinction in pyroxene. Shock effects on the paleomagnetism of Lonar Crater (Cisowski, 1975; Poornachandra Rao and Bhalla, 1984; Louzada et al., 2008) are subtle and consistent with low to moderate shock levels.

At the surface, the most dramatic evidence for the impact shock is the presence of impact spherules. Around the eastern and western rim of Lonar Crater, Nayak (1972) identified sculpted, vesicular impact glasses with diameters 0.1–4 cm and densities 1.32–2.65 g cm^{-3}. Fredriksson et al. (1973a) also found small (0.1–3 mm) flow-banded, teardrop-shaped spherules and larger (10- to 15-cm-diameter) pieces that wrap around underlying clasts like the Flädle of Ries crater (Hörz, 1965). Sengupta et al. (1997) describe spherule-rich layers 5 cm below modern alluvium from trenches along the western and southeastern crater rim. The chemistry and internal structures of the impact glasses have been described in detail (Fredriksson et al., 1973a, 1973b; Kieffer et al., 1976; Morgan, 1978; Fredriksson et al., 1979; Osae et al., 2005; Chakrabarti and Basu, 2006; Son and Koeberl, 2007). Glass fragments significantly enriched in silica and sodium compared to the Poladpur Formation of the Deccan basalts (Murali et al., 1987; Chakrabarti and Basu, 2006) are associated with abandoned kilns and fused bricks (Fig. DR3 [see footnote 1]) and are likely produced by humans during the brick firing process (Fudali and Fredriksson, 1992).

Recently, the relatively young age for Lonar Crater formation has been confirmed. The Deccan basalts at Lonar Crater were erupted during paleomagnetic Chron 29R (Vandamme et al., 1991; Louzada et al., 2008, and references therein), suggesting a K/Ar emplacement age of 64.7 ± 0.6 Ma (Chenet et al., 2007), recently recalibrated to ca. 65.1 Ma (Kuiper et al., 2008). In contrast, Lonar Crater formed between 15 and 67 ka (Fredriksson et al., 1973a; Fudali et al., 1980; Taiwade, 1995; Ghosh, 1996; Sengupta et al., 1997; Ghosh, 2003; Storzer and Koeberl, 2004), as discussed in more detail below.

RESULTS

Digital Topographic Survey

With 135 m of relief from raised rim to lake level, Lonar Crater is the most significant topographic feature in this otherwise flat region of the Deccan Plateau. We developed a DEM by collecting 64,000 spatial data points using consumer-grade, handheld global positioning system (GPS) units (Garmin 60c and 76c) while walking geologic traverses in and around the crater (Figs. 2, DR4, and DR5; the full DEM is available in the GSA Data Repository [see footnote 1]). The coordinates of the crater center are 657867E, 2209626N Universal Transverse Mercator (UTM; WGS84, zone 43) or 76.50°E, 19.97°N, and the present crater rim crest radius is 940 ± 25 m. Note that our measured crater

[1]GSA Data Repository item 2009131, additional field photographs, crater profiles and maps, and a digital elevation model available for download, is available at http://www.geosociety.org/pubs/ft2009.htm or by request to editing@geosociety.org.

radius is slightly larger than the 915-m average radius previously reported (Fredriksson et al., 1973a; Fudali et al., 1980).

We found that the GPS units were most accurate when left on and collecting data the entire day; therefore, the units were only shut off at night. In order to determine absolute accuracy and reproducibility of our spatial GPS data set, we surveyed six specific landmarks (for <5 seconds each) once or twice a day for three weeks (over the course of two years). Histograms of GPS deviation from the mean are shown in Figure DR6 [footnote 1]. We found that the 1σ error on our GPS measurements averaged 1.5 m east-west, 1.9 m north-south, and 2.4 m in elevation. We evaluated the precision in our measurements by comparing a surface gridded with 400 GPS data points to a surface gridded with 400 data points acquired using a Leica TCR303 total station with nominal 2 cm precision over the same 1600 m^2 area on the eastern crater rim. Nowhere did the difference between the two surfaces exceed 5 m. Furthermore, 75% of the area showed <2 m discrepancy between the GPS-derived surface and the total station derived surface; large errors were isolated to regions that had a dearth of TCR303 data because they were not in line of sight to the total station. Dual GPS and total station measurements of specific landmarks confirmed the observation that GPS precision was ±1 to ±3 m in x, y, and z directions. The DEM was computed by applying a universal Kriging gridding algorithm (Cressie, 1993) to the GPS data. In regions covered by a favorable density of points, DEM precision is ±5 m or better. For reference, the DEM is five times more precise than ASTER satellite–derived DEMs and not subject to elevation errors caused by vegetation canopy.

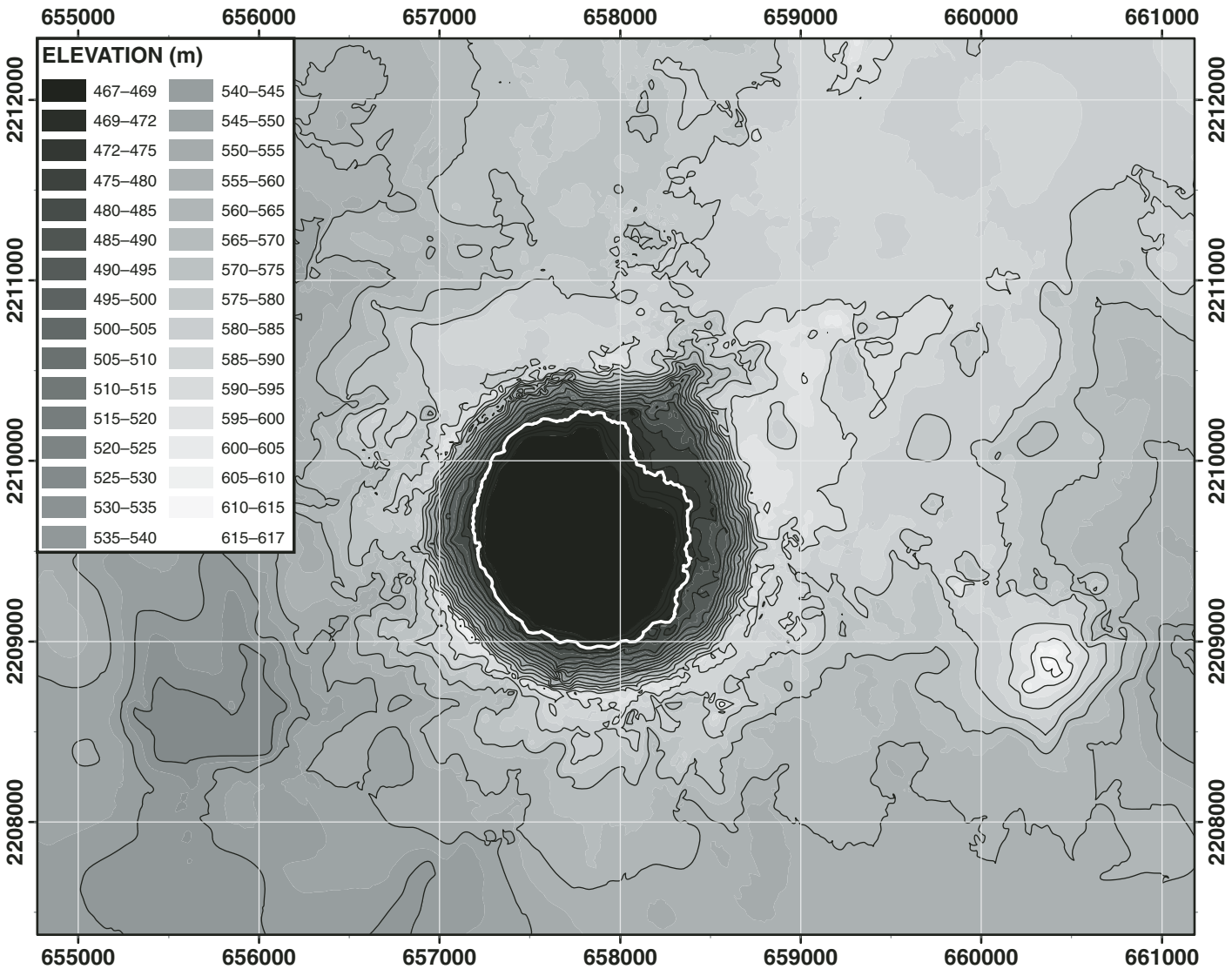

Figure 2. Global positioning system (GPS)–derived digital elevation model for Lonar Crater. The filled contour map is derived from 64,000 individual GPS measurements (see Fig. DR4 [footnote 1]). Bathymetric data in Lonar lake are derived from contours presented by Nandy and Deo (1961), and the 2006 lakeshore (white line) is traced from the Quickbird satellite image (Fig. 1). Kalapani and Lonar town lakes do not have bathymetric data but are very shallow, and we approximate them as flat surfaces. Thin black lines delineate 10-m contour intervals. Easting (655000–661000) and Northing (2208000–2212000) coordinates are in Universal Transverse Mercator (UTM) (WGS84) meters. Color version in GSA Data Repository [footnote 1].

Volcanostratigraphy of Deccan Trap Target Rocks

Within the crater, there are six 10- to 25-m-thick basalt flows (Tf0–Tf5; Figs. 3, 4, and DR7 [footnote 1]), all of which are characterized by broad flow fronts and nearly flat upper surfaces capped by discontinuous flow-top autobreccias (Figs. 5A and 5B). Within a single flow, an internal stratigraphy is usually developed that begins with thin, sporadically developed, fine-grained pipe-vesicle basalt (Figs. 5G and 5H), followed by dense, nonvesicular, jointed and sometimes flow-banded basalt (Figs. 5E and 5F), which passes upward into vesicular, and sometimes amygdaloidal, fine-grained basalt that is often deeply weathered (Nayak, 1972; Fudali et al., 1980). The dense, nonvesicular parts of Tf4 (at Penpalmer Dam) and Tf5 (at Durga Devi Hill Quarry) have porosities (±1σ) of 3.9 ± 1.6 (n = 5) and 3.2 ± 1.9 (n = 5) % and densities (±1σ) of 2.93 ± 0.03 (n = 5) and 2.94 ± 0.04 (n = 5) g cm^{-3}, respectively, similar to that found by Fudali et al. (1980). The top of Tf4 has sporadically developed microcolumnar basalt (Figs. 5C and 5D), which is particularly well developed at Durga Devi Hill Quarry (Fig. 1B). The microcolumns display disordered 90°–90° angles at the true flow top, and become more widely spaced and better ordered 60°–120° hexagonal and pentagonal cracks at depth, consistent with sequential fragmentation during downward propagation of the cooling front (Jagla and Rojo, 2002). Both columnar-jointed and vesicular autobreccia flow tops are very permeable and usually deeply altered. When the alteration front penetrates more than a few centimeters, a fine red powdery paleosol (often referred to as "red bole") is commonly developed between basalt flows (Figs. 5C and 5D).

Although previously interpreted as aa flows (Dube and Sengupta, 1984; Ghosh and Bhadur, 2003), the lack of prominent flow bottom breccia, the lack of mixing between flow-top breccias and flow core units, and the sheet-like geometry of flows over several kilometers indicate greater affinities to typical inflated pahoehoe (Duraiswami et al., 2003). The northeast and east regional elevation highs (Fig. 2) are coincident with the preservation of a thicker basalt stack, capped by severely weathered outcrops of what we tentatively interpret as a seventh basalt flow (TF6; Figs. 3 and 4). However, we cannot rule out the existence of additional, recessively weathering vesicular basalt units between Tf5 (which defines the rim of the crater and the quarry on the east side of Durga Devi Hill) and Tf6, which caps the top of Durga Devi Hill (Fig. 1). Based on the available data, we map seven flows between the crater floor and the top of Durga Devi Hill and assume that the North Quarries preserve the Tf5–Tf6 contact.

Impact-Induced Deformation of Target Basalt Flows

Folding

The raised crater rim and exposed crater wall are composed of upturned to overturned basalt stratigraphy, typically dipping 10°–30° out from the crater (Fig. 6B). Along the rim crest, Tf5 is recumbently folded and variably brecciated, with semi-intact beds preserving a reverse basalt stratigraphy (Figs. 6 and DR8 [footnote 1]). The slope of the uppermost canyon wall is usually

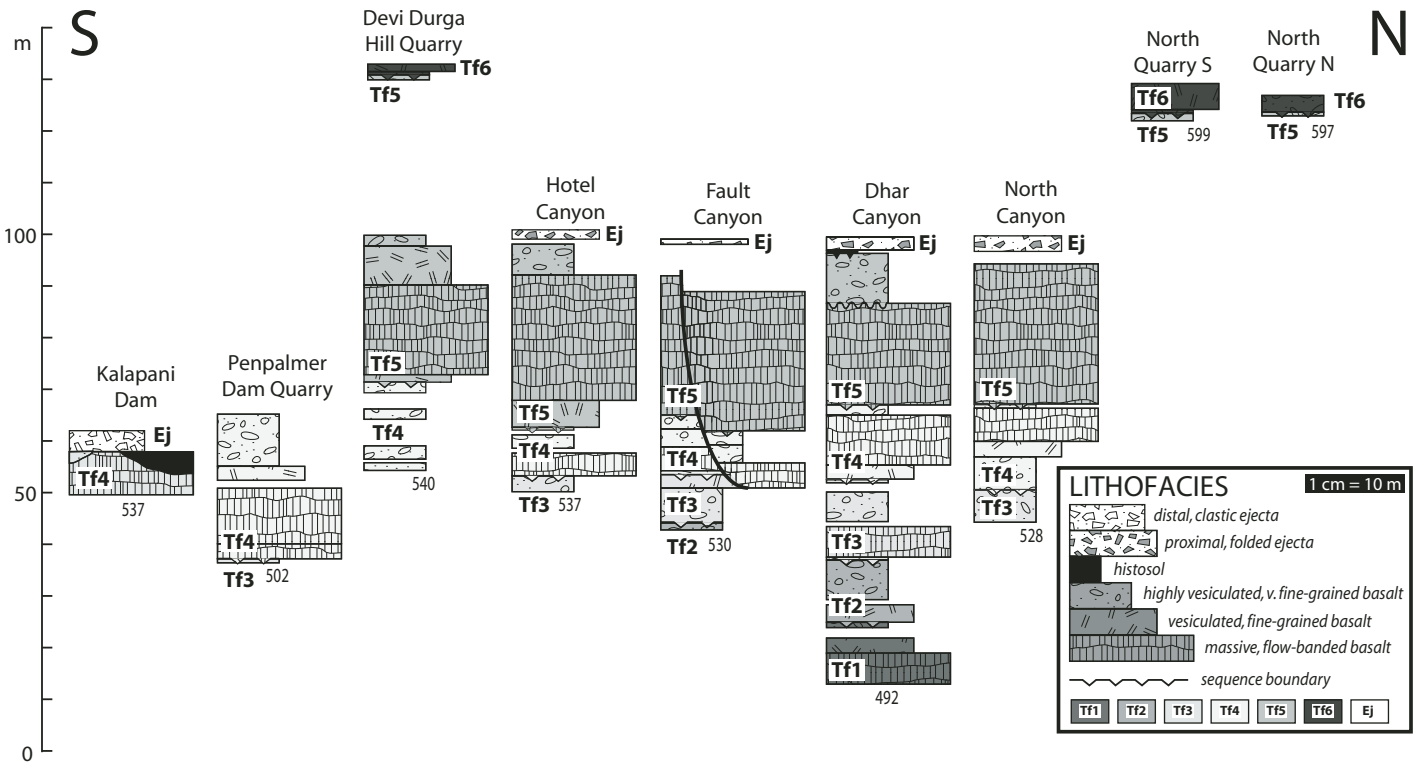

Figure 3. Basalt stratigraphy from crater walls (Hotel Canyon, Fault Canyon, and Dhar Canyon) and surroundings (Penpalmer Dam Quarry, Kalapani Dam, Durga Devi Hill Quarry, North Quarry South, and North Quarry North). Flow 0 (Fig. 4) is present as isolated outcrops near the bottom of the crater and is not included in measured stratigraphic sections. Elevations in meters (not corrected for rim uplift) are marked at the base of each section; section locations are marked on Figure 1B, except for Penpalmer Dam Quarry, which is southeast of the Figure 1B map area. Basalt and ejecta lithofacies are color coded by relative age. Universal Transverse Mercator (UTM) locations are provided in Table DR1 [footnote 1]. Color version in GSA Data Repository [footnote 1].

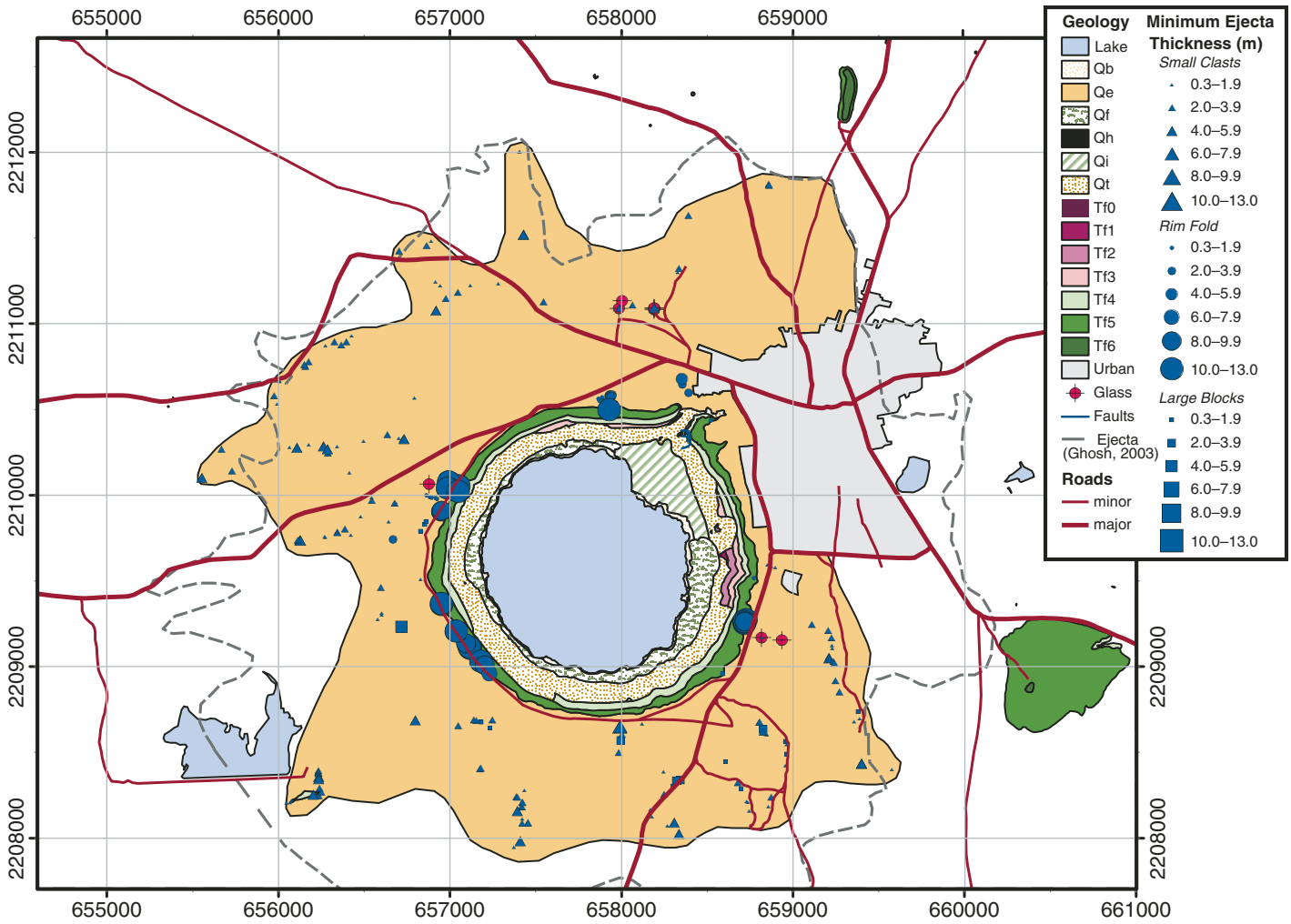

Figure 4. Geological map of Lonar Crater. Blue symbols are shaped and sized to reflect the type and thickness (meters), respectively, of impact ejecta at specific outcrops. Magenta circles correspond to glass impact spherule localities. The dashed gray curve outlines the edge of the continuous ejecta blanket determined by Ghosh (2003). Quaternary units: Qb—beach, Qe—ejecta, Qf—forest, Qh—histosol, Qi—irrigated alluvial fan, and Qt—talus. Easting (655000–661000) and Northing (2208000–2212000) coordinates are in Universal Transverse Mercator (UTM) (WGS84) meters.

greatest where the rim-fold hinge is preserved and vertical flow bands in massive basalt from Tf5 form a dip slope (Fig. 6C).

The recumbent limb of the rim-fold also is parasitically folded around subhorizontal, noncylindrical fold axes that are concentric to the crater rim (Fig. 6). These parasitic folds are open and upright, and resemble wrinkles in a carpet. Although parasitic fold hinges are not observed, flow banding in massive basalt blocks 1–20 m in diameter delineate the fold limbs. In Figure 7, measurements of the flow-banding dip azimuths fall into three groups: uplifted basalt flows with azimuths pointing away from crater center (solid circles), overturned rim-fold blocks with azimuths pointing toward and away from crater center (squares), and jumbled ejecta blocks with more widely scattered azimuths (open circles).

In a companion paleomagnetic study, Louzada et al. (2008) conducted fold tests (McElhinny, 1964) at four locations around the crater rim (east, south, northwest, and west). They found that the crater rim-fold can be approximated as a localized cylindrical horizontal fold with a fold axis parallel to the rim, this result confirms our assumption that flow banding in massive basalt (Figs. 5E and 5F) records paleohorizontal. Two sites (eastern and southern rim) pass a complete fold test at the 95% confidence level, where the clustering of magnetization vectors increases upon 100% unfolding. The positive fold test indicates that the primary early Tertiary (Chron 29R) remanent magnetization in the basalts is preserved, and that the primary magnetic vectors are folded.

Elsewhere, the assumption of cylindrical folding is invalid. The paleomagnetic data instead support the field observation that during rim folding, tear zones developed due to dilation of the recumbent limb, and breccia blocks experienced substantial (30° or more) vertical axis rotation (Louzada et al., 2008). The western rim breccia blocks are so jumbled that they pass a conglomerate test for randomness in paleomagnetic directions, indicating that rim-folding was locally chaotic. Note that pseudo-concentric fractures in the schematic drawings of Figures 6B and 8A are meant to depict pervasive brecciation, not specifically observed concentric fractures.

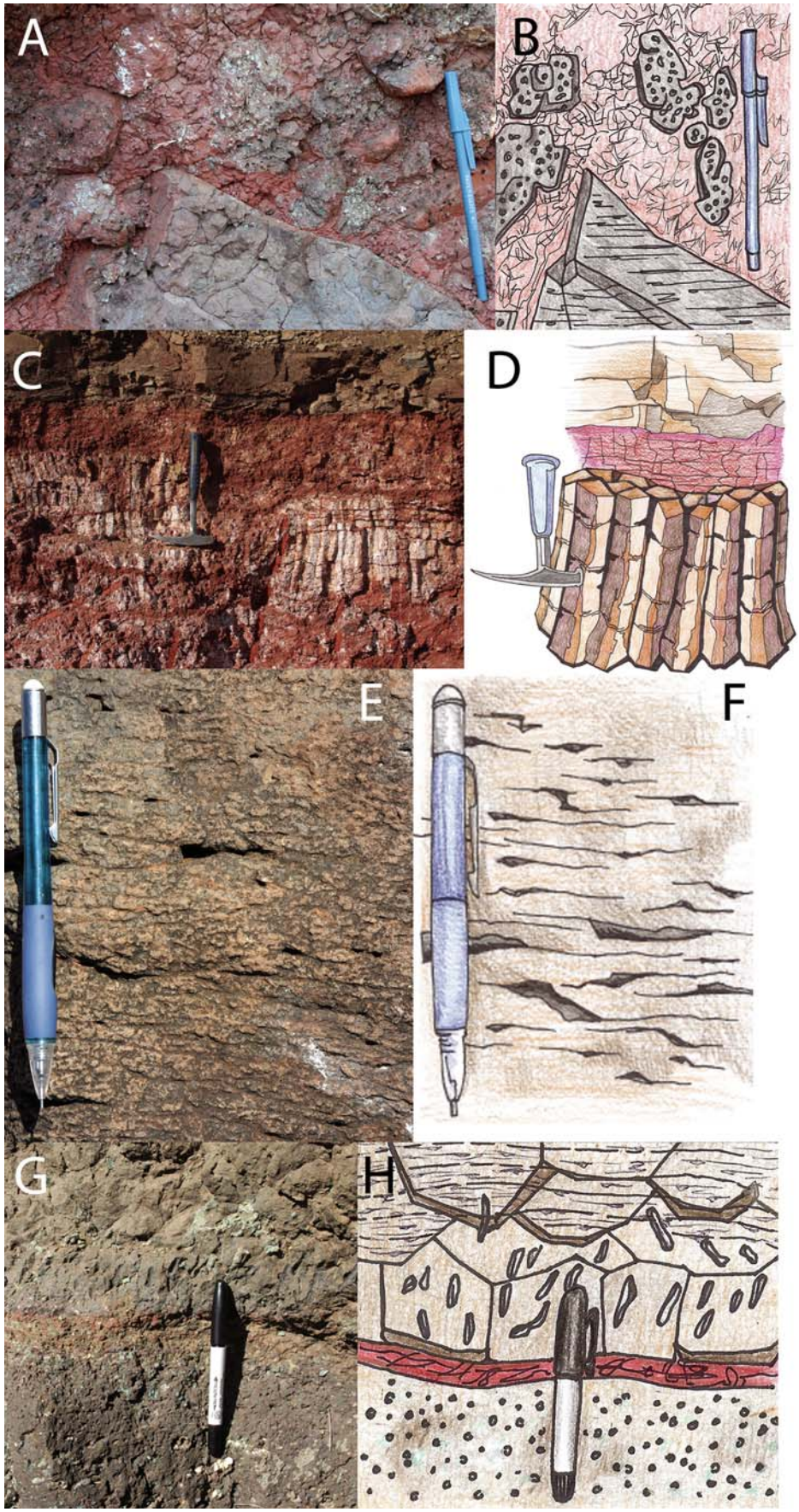

Figure 5. (A, B) Flow-top vesicular autobreccia developed on the top of Tf4 in Dhar Canyon (Universal Transverse Mercator [UTM]: 658335E, 2210507N). (C, D) Columnar joints developed in the upper meter of Tf4 below massive basalts at the base of Tf5 at Durga Devi Quarry (UTM: 660753E, 2209124N). Both autobreccia and columnar jointing increase the permeability of basaltic flow tops and lead to preferential development of ferruginized paleosols ("red bole"). (E, F) Flow banding in massive basalt associated with shearing of microvesicles during lava flow along paleohorizontal (UTM: 657045E, 2210044N). (G, H) Vesicular Tf3 flow, ferruginized at the top and overlain by massive Tf4 with well-developed pipe vesicles at North Canyon (UTM: 657580E, 2210407N). Amygdules, present in some of the vesicles are green zeolite, white calcite, and/or translucent gray quartz (based on preliminary microprobe analysis).

Fracturing and Faulting

Although dilation, fracture, and vertical axis rotation are all inferred from field and paleomagnetic analysis of the rim-fold, no tear zones are observed directly as measurable displacement between two adjacent rocks. Even in Dhar Canyon (Fig. 1B) where a large gash in the crater wall is occupied by a perennial spring, there is no significant displacement of the basalt flows. Kumar (2005) describes a network of radially striking, steeply dipping fractures in massive Tf4 and Tf5 of the crater wall. Although we do not have enough data to question Kumar's (2005) result, the high-angle fractures that we typically observe are not consistently radial to the crater center and are similar to the spaced 60–120 and 90–90 joint sets common in undeformed massive basalt outside the crater (e.g., Tf4 in the foreground of Figs. 9A and 9B).

Kumar (2005) also describes a network of conical fractures in Tf4 and Tf5 of the upper crater wall that dip more steeply out of the crater than the bedding planes. However, we did not find outcrops where quaquaversal fractures cut across flow banding at a significant angle. Instead, we found that flow banding is easily mistaken for fractures and that steeper quaquaversal dips in the upper crater wall are associated with rim-folded flow banding, not a conical network of cracks.

The most prevalent fault deformation that we observe directly is layer-parallel slip along the Tf4–Tf5 contact on the crater wall (Figs. 8 and DR9 [footnote 1]). Outside the crater, the Tf4 flow top is often a well-developed, ≤1 m thick

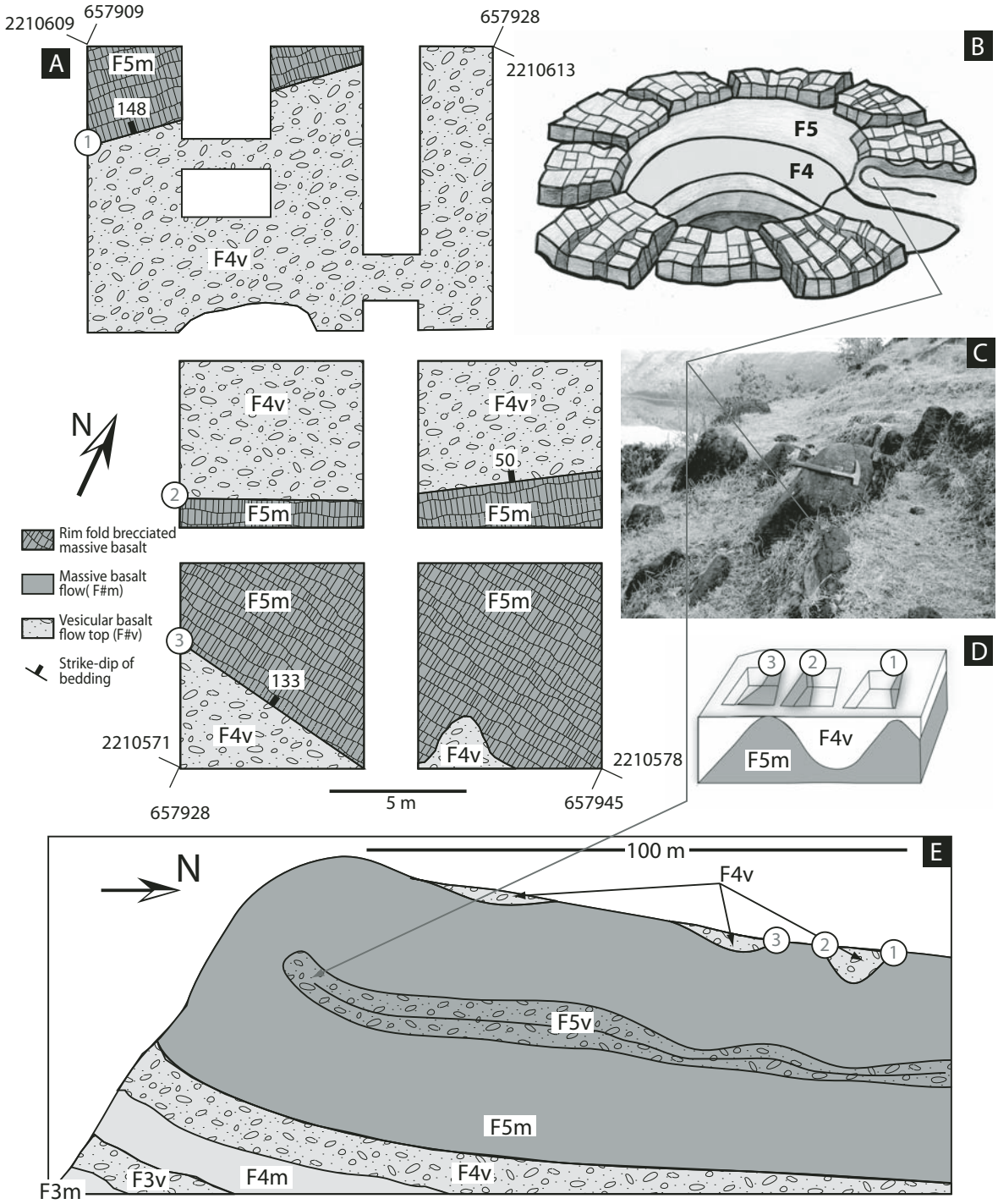

Figure 6. (A) Geological map (plan view of [E]) of the rim-fold where it is intersected by five excavated pits associated with an abandoned telecom office building project. Corner coordinates for surveyed telecom pits are reported in meters (Universal Transverse Mercator [UTM], WGS84). White area refers to grassy alluvium where there are no excavations. (B) Schematic drawing of Lonar Crater, emphasizing the geometry of the rim-fold breccia, parasitically folded around rim-concentric fold axes, with individual breccia blocks progressively rotated around vertical axes with distance away from the crater and/or toward cryptic tear zones. Note that the pseudo-concentric fractures in the rim-fold ejecta are meant to depict pervasive brecciation, not specifically observed concentric fractures. (C) Example of preserved fold hinge in crater rim, with massive flow banded basalt in foreground dipping steeply into the crater (also see Fig. DR8 [footnote 1]). Contacts 1, 2, and 3 from (A) are indicated in (D), a very schematic drawing of three of the excavation pits showing only F5m for simplicity (white area is a combination of F4v and colluvium), and (E) a cross section through the north wall of Lonar Crater (topography and surface contacts are drawn accurately and to scale). The rim-fold preserves a brecciated, parasitically folded, reverse basalt stratigraphy, with vesicular Tf4 flow-top upside-down on top of massive lower Tf5. Color version in GSA Data Repository [footnote 1].

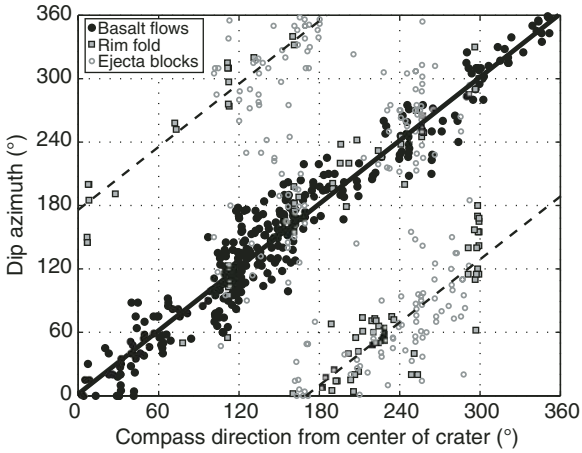

Figure 7. Dip azimuth of flow banding in massive basalt from intact lava flows in the crater wall, rim-fold, and ejecta blocks. Crater wall basalts dip radially outward from the crater and can be fit with a line of slope 1 with $r^2 = 0.9$. Rim-fold blocks have populations dipping radially out from the crater (solid linear regression), as well as radially into the crater (dashed linear regressions), suggesting parasitic folding around subhorizontal, rim-concentric fold axes (see Fig. 6). Ejecta blocks around the fringe of the rim-fold also show rim-concentric fold axes, but with relatively more azimuthal scatter associated with vertical axis rotation near tear zones. Dip information is derived from flow banding in massive basalts or contacts between flow units.

zone of columnar joints and deep chemical alteration (Fig. 5C). Inside the crater, the Tf4–Tf5 contact is a knife-sharp, brick-red–colored layer (Fig. 8A) with slickenslides that indicate motion of the hanging wall (Tf5) up and into the crater (Fig. 8G). This faulting is consistent with layer-parallel slip along a weak contact during recumbent folding of the crater rim (Fig. 8B).

At Fault Canyon (Fig. 1B), a second, younger set of faults is apparent (blue lines in Fig. 4, and Kumar (2005) Fig. 1B). It is the only location where we observe unequivocal large-scale normal faults. Two coherent slump blocks (b and c in Figs. 8A and 8B) slid into the crater on steep normal faults that cut across and displace the Tf4–Tf5 layer-parallel slip fault. These en echelon normal faults decapitate the rim-fold. Unfortunately, the rim-fold hinge is preserved only around 10%–15% of the crater rim. However, landslide scars and rubble piles are abundant on the crater wall.

Geologic Mapping of the Ejecta Blanket

Away from the crater edge, the rim-fold breccia pinches out into a thin (up to 7 m thick) but continuous blanket of impact ejecta (Fig. DR10 [footnote 1]). This transition is apparent as the prominent change in slope and color at the edge of the white rim-fold proximal ejecta and cultivated distal ejecta in the satellite image (Fig. 1B). Due to extensive land modification by farmers, it is difficult to say whether the apparent scalloping (sinuousity) in the distal edge of the modern ejecta blanket is a primary depositional feature (Fig. 4). However, existing sketches and maps (Fudali et al., 1980; Ghosh, 2003) of the crater ejecta, albeit different in detail from our observations, depict a similarly scalloped termination of the continuous ejecta blanket and suggest that the scalloping does not owe its origin to farm modification of the past 20 years. Note that the trace of the terminus of the ejecta blanket in Figure 4 published by Ghosh (2003) is based on the same field work as Fudali et al. (1980) in the 1970s.

In distal localities such as Kalapani Dam Quarry (Figs. 9A–9D) and the Road-to-Kinhi Quarry (Figs. 9E and 9F), undeformed subhorizonal basalt flows are overlain by an unsorted and unstratified ejecta unit dominated by massive basalt clasts usually ≤2 m in diameter (but see Figs. 9G and 9H) and powdery, deeply altered vesicular basalt clasts in a coarse-grained matrix. Because of the similarity in composition, it is usually difficult to determine with confidence what percent of the matrix is reworked alluvium and soil and what percent is primary ejecta, except where distinctive substrate units are present. A black, muddy histosol up to 2 m thick, with distinctive white calcified root casts, is common in natural depressions within the flow-top of Tf4 (Figs. 9A–9B and DR10) and is disconformably overlain by the ejecta. Modern analogues to this muddy histosol form today in topographic depressions filled with grassy wetlands.

In some instances, blocks within the ejecta blanket penetrate the underlying histosol, and the same histosol unit is mobilized into impressive flame structures that penetrate up into the ejecta (Figs. 9E and 9F). More common than the large penetration stones and histosol flame structures are an abundance of cm-size rip-up clasts of histosol that are incorporated into the debris flow, and cm-size ejecta clasts that penetrate up to 30 cm into the histosol (Figs. 9C and 9D). Small histosol clasts may be found within the ejecta up to 0.75 m above the ejecta-histosol contact. However, we did not find any histosol clasts in ejecta more than 10 m away from an observed outcrop of histosol.

Minimum ejecta thicknesses (Fig. 10) were determined by measuring the thickness of ejecta above the basement surface. The basement surface was defined at the rim by the core of the rim-fold and elsewhere by the sharp contact between the surrounding basalt flow structures and the debris flow layer. All ejecta thickness measurements are considered minimum values, as some erosion has occurred throughout the ejecta blanket and, in some cases, the basement rock level was not exposed. In locations proximal to road or farm excavations, we did not measure ejecta thickness unless the ejecta was directly overlain by Quaternary bedded alluvium deposits (e.g., Figs. 9C and 9D) that predate any accumulated anthropogenic debris. Note that Quaternary alluvium deposits were not included in the minimum thickness measurements. The symbols in Figure 10 reflect three categories of clast sizes: (1) circles—rim-fold material with brecciated inverted stratigraphy (Fig. DR8 [footnote 1]); (2) squares—large (m-scale) blocks with a smaller volume fraction of finer grained matrix (e.g., Fig. DR10C [footnote 1]); and (3) triangles—small clasts (typically <1 m) in a coarse matrix (Figs. DR10D and DR10E [footnote 1]). Note the abrupt transition between the rim-fold and the ejecta debris flow. Clasts within the ejecta debris flow are randomly oriented and pass a paleomagnetic conglomerate test (Louzada et al., 2008).

The observed minimum thicknesses for the ejecta blanket show a strong departure from the expected ballistic power-law thickness profile for small craters (McGetchin et al., 1973; Kring, 1995). Instead, at Lonar, the ejecta thickness decays rapidly within 1.2 crater radii and is thicker than expected between 1.5 and 3 crater radii. There is no significant azimuthal or regional slope dependence on the ejecta blanket profile (Fig. DR11 [footnote 1]); the terminal rampart appears in all directions, including upslope. Note that we were unable to reproduce the exact ejecta thickness measurements at locations reported in Ghosh (2003).

In order to quantify the brecciation in the ejecta debris flow, we measured the bulk density of ejecta deposits in the field. Bulk density measurements were conducted at three locations to the northwest of the crater at distances of 1.2, 1.4, and 2.2 crater rim radii from the crater center. Using a portable hanging scale and a measuring vessel of known volume, we determined the mass of material in a 2–3.5 L hole dug into the ejecta blanket. With increasing distance from the crater center, the average

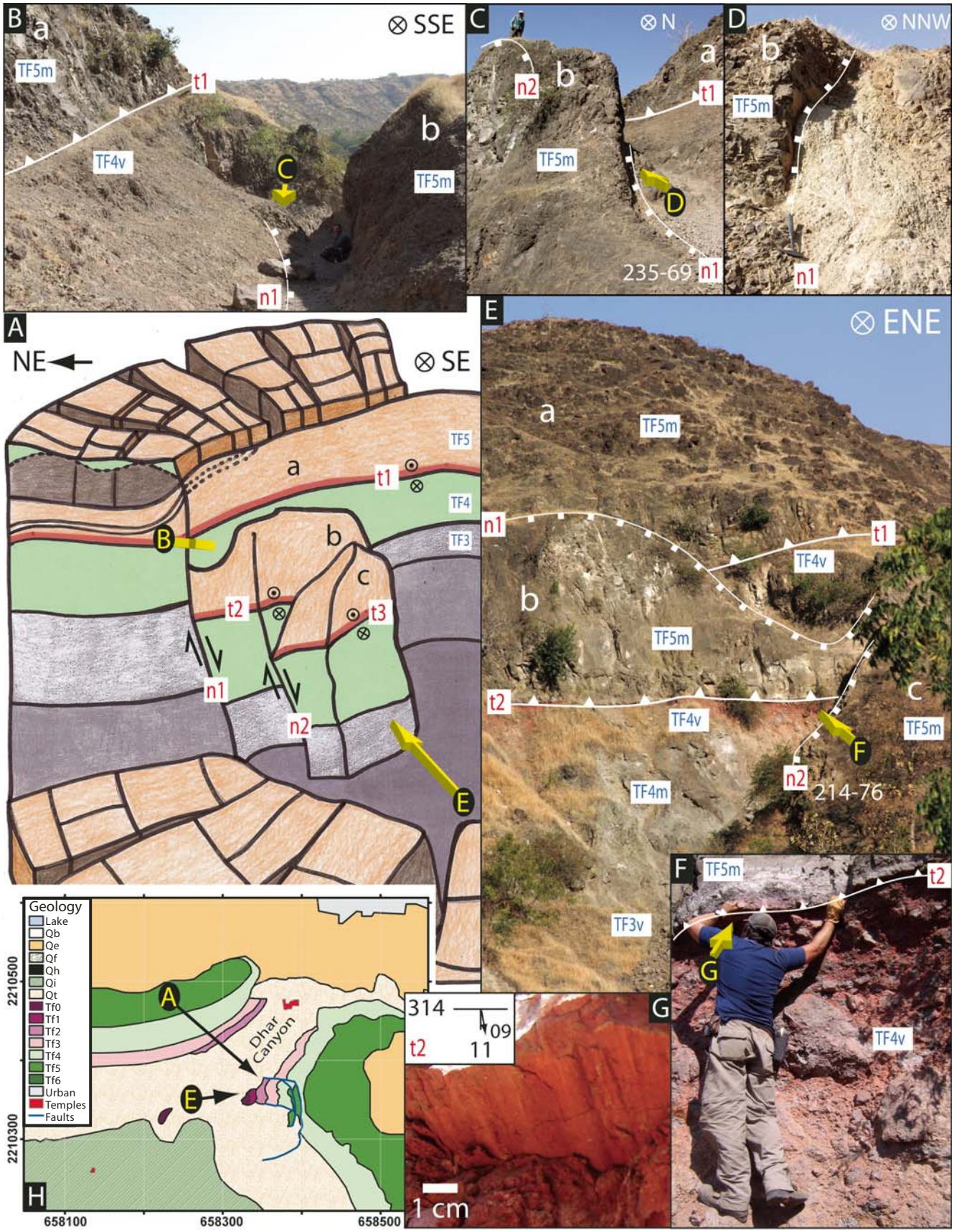

Figure 8.

Figure 8. Two generations of faults are preserved in Fault Canyon (Fig. 1B). Panel (A) is a schematic drawing of the faulted region, sketched as if the artist were sitting on the crater rim on the northwest side of Dhar Canyon (H; refer to legend from Fig. 4). The older generation of fault is depicted in (A) as the sharp red line tracing the primary volcanic contact between vesicular and brecciated flow 4 (Tf4v) and basal massive flow 5 (Tf5m). The fault is best exposed along the "n2" normal fault on block "b," as shown in (E; vertical scale is ~80 m) and zoomed-in on in (F; Maloof for scale; Universal Transverse Mercator [UTM]: 658393E, 2210326N). A close-up of the fault in (G) reveals slickensides that indicate hanging wall–into-the-crater (thrust) motion essentially parallel to the dip of the local bedding. The strike and dip of the fault plane and flow boundary are 314 and 11, respectively, with the slickensides plunging 9°. Some of the brecciation apparent in Tf4v may be associated with the faulting, although primary autobrecciation of this flow top is apparent in North, Dhar, and Hotel Canyons (but not at Durga Devi—Fig. 5C). The once continuous thrust fault is displaced into "t1," "t2," and "t3" by a younger generation of listric normal faults or slumps, labeled "n1" and "n2." Normal fault "n1" is shown in (B—Soule for scale), (C—Soule for scale), and (D—hammer for scale) and juxtaposes Tf5m in block "b" against Tf4v in block "a" along an active human footpath. The trace of "n1" is irregular, but in (C), the dip direction–dip is 235–69. In (E), the trace of "n2" separates blocks "b" and "c," has dip direction–dip of 214–76, and occupies the gully in which we measured the Fault Canyon stratigraphic section in Figure 3. In each panel labeled A–H with a white capital letter in a black rectangle, the "⊗" indicates the cardinal direction in which the camera is oriented; yellow or black arrows indicate the viewing direction represented in the panel indicated with the yellow capital letter in a black oval; each fault block is labeled with a lowercase "a," "b," or "c"; each fault trace is labeled with red letters "t" for thrust and "n" for normal fault; white lines with triangles are thrust fault traces, and white lines with squares are normal fault traces; displacement on the faults in (A) is denoted with opposing half arrows or opposing circled circles (⊙) and circled "x's" (⊗); each lava flow is labeled with blue letters in a white box. Note: the colors associated with Tf3–Tf5 are not the same in (A) and (H).

densities (±1σ) were found to be 1.97 ± 0.50 (n = 3), 2.39 ± 0.11 (n = 3), and 2.14 ± 0.31 (n = 2) g cm^{-3}. Using original bulk densities of 2.9 g cm^{-3}, the porosity in these locations in the ejecta ranges between 18% and 32%.

The excellent preservational state of the ejecta blanket is supported by the patchy occurrence of impact glass and spherules, and a high density of ejecta blocks. In some areas, ejecta blocks have been cleared for farming, particularly to the west and south. The size distribution of ejecta blocks is spatially heterogeneous with large boulders found throughout the ejecta blanket (Fig. DR10 [footnote 1]). Recent reports of heterogeneous hydrothermal alteration in the rim-fold breccia (Newsom et al., 2005) are not supported by this work. Our field observations show that previously interpreted altered ejecta (e.g., at the Telecom Pits—Fig. 6) are highly comminuted materials originating from autobrecciated, vesicular or amygdaloidal basaltic flow tops weathered prior to the impact event. In further support of our interpretation, at least one comminuted ejecta zone contains well-preserved impact glasses and sub-mm glass spherules (UTM: 658817E, 2209170N).

Impact glass is most abundant in the rare regions of the crater rim that appear to be unaltered by human activity or mass wasting. We collected hundreds of samples of basaltic impact glass (Fig. 11) from the southeastern and northwestern crater rim (Fig. 4), and from the southwestern and southeastern rim of Little Lonar depression (Fig. 12). Many of the smaller melt glasses are aerodynamically and rotationally sculpted and must have solidified during flight. Circular and elliptical vesicles are common, particularly toward the center of glassy objects. Weiss et al. (2007) conducted demagnetization and rock magnetic measurements on more than 60 sculpted impact glasses. They found that the glasses are inefficiently magnetized and have magnetic remanence that was blocked while the samples were rotating, consistent with cooling and solidification while airborne.

Little Lonar

Little Lonar (a.k.a. Amber Lake, Master, 1999) is an elliptical depression ~700 m NNE of Lonar Crater rim (center, UTM: 658122E, 2211223N) currently used for chick pea farming. The depression has a diameter of ~300 m and wall deposits up to >12 m thick (Fig. 12). Fredriksson et al. (1973a) and Fudali et al. (1980) suggested that Little Lonar is a second impact crater formed by a fragment of the larger bolide that was responsible for Lonar Crater.

The southern wall of Little Lonar is composed entirely of unsorted ejecta blocks of massive basalt ≤1.5 m in diameter within a coarse-grained matrix. We dug trenches at the base of the wall deposit to determine a minimum ejecta thickness for the Little Lonar "rim" (Fig. DR13). However, even at 12.4 m, our trench did not encounter a basal, intact basalt flow. The recovered stratigraphy has 4.8 m of ejecta without glass, overlain by 2.8 m of ejecta containing locally abundant fragments of impact glass (including aerodynamically sculpted forms), overlain by 5.2 m of ejecta without glass and topped by 0.3 m of colluvium.

If Lonar and Little Lonar were a double impact, their bolides would have struck nearly simultaneously. Because of its significantly smaller size, Little Lonar would have finished forming and laid down most of its ejecta blanket before the arrival of the ejecta curtain from its larger neighbor and subsequent deposition of the spherules. For reference, typical transient crater formation time scales for 1.7- and 0.3-km-diameter craters in a hard rock struck by an asteroid are ~6 and 2 seconds, respectively (Melosh, 1989; Melosh and Beyer, 1998). The ballistic flight time from near the center of Lonar to Little Lonar is around 17 s. Hence, we would expect to find the primary ejecta blanket deposited on top of Little Lonar's Crater rim. The observation is just the opposite. The spherule-rich layer is embedded beneath several meters of debris, whereas in other locations around Lonar Crater, impact glass from atmospheric fallout is concentrated in the upper few centimeters of the ejecta. Therefore, we suggest that the upper 7.8 m of ejecta at Little Lonar is composed of dirt and boulders that farmers piled up around a smaller preexisting depression, rather than ejecta from a second crater. The remaining 5.0 m thickness of primary ejecta is consistent with other ejecta thickness observations from around Lonar Crater (Fig. 10).

^{14}C Data from Pre-Impact Paleosol Organic Matter

Interpretations of the geometry and preservation of the ejecta blanket, the magnetic signature of the ejecta and impacted basalt, and slope evolution of the crater wall require an accurate age for the impact event that formed Lonar Crater. Unfortunately, the young age and lack of suitable mineralogies make direct determination of the age of impact very difficult. Published ages range from 15.3 ± 13.3 ka from fission-track counts in impact glass (Storzer and Koeberl, 2004), to 45–67 ka, using the thermoluminescence method on impact glass (Sengupta et al., 1997). Unpublished radiocarbon dating of organic

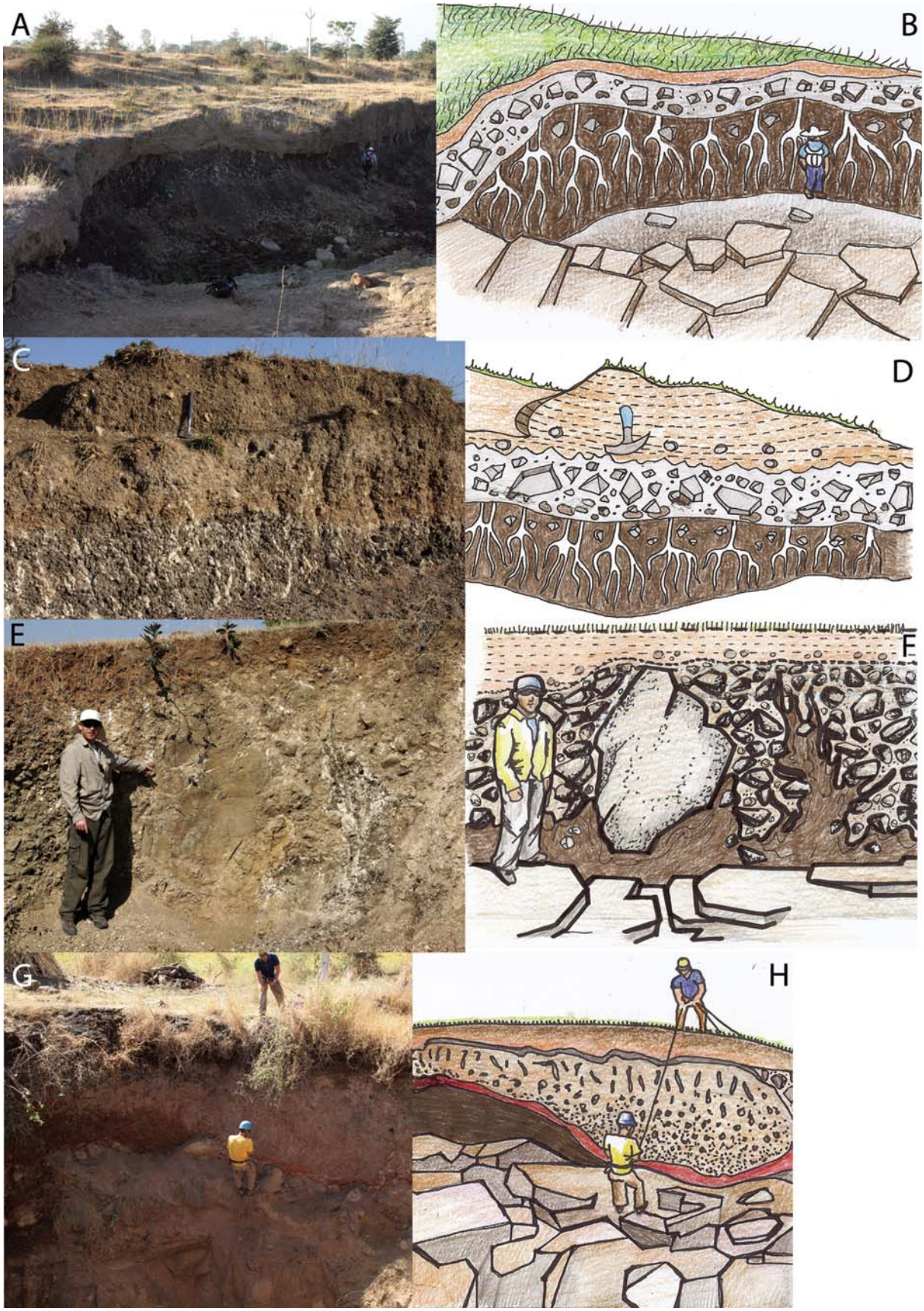

Figure 9.

Figure 9. (A, B) Vertically jointed massive basalt of Tf4 occupies the foreground in this image from Kalapani Dam (Universal Transverse Mercator [UTM]: 656085E, 2208231N). Black histosol with white calcified root casts fills a natural depression in the pre-impact basalt landscape. The light-brown layer on top of the histosol is unsorted impact ejecta consisting of ≤1.5-m-diameter massive basalt clasts, powdered and deeply altered vesicular basalt clasts, and reworked ≤0.15-m-diameter chunks of underlying black histosol localized in the lowermost 30 cm of the ejecta pile adjacent to histosol outcrops. The impact ejecta layer truncates the root casts in the underlying histosol. (C, D) At Kalapani Dam (UTM: 656085E, 2208231N), the succession of black histosol with white calcified root casts overlain by light-brown ejecta is in turn truncated by darker brown, modern cross-bedded alluvium. (E, F) At the quarry on the road to Kinhi (UTM: 656126E, 2209737N), Soule points to a 2-m-diameter massive basalt clast in the ejecta unit. Basalt clasts impinge on the underlying histosol, and large clasts often cause fluidized injections of histosol into the ejecta (right-hand side of image). (G, H) Swanson-Hysell is belayed by Maloof into a new well (UTM: 658857E, 2211813N). At this location, a 9 × 2 × ? m clast preserves an intact, but upside-down progression from massive flow-banded to vesicular and autobrecciated basalt and is surrounded by finer ejecta. The ejecta overlie a discontinuous layer of histosol and ≥5 m of undeformed massive Tf5 basalt stratigraphy.

materials from drill cores in the lake sediments imply approximate lower limit ages between 15 and 30 ka (Sengupta and Bhandari, 1988).

We collected histosols and organic-rich swamp muds for radiocarbon measurements beneath the distal ejecta blanket at: three locations at Kalapani Dam (UTM: 656087E, 2208221N; Figs. 9A–9D), two locations at the Road-to-Kinhi Quarry (UTM: 656343E, 2209784N; Figs. 9E and 9F), and one location at a large pit preserving 0.3 m of muddy histosol overlain by 0.7 m of ejecta with histosol clasts, in turn overlain by 3.8 m of clean ejecta (UTM: 656919E, 2211078N). We removed macroscopic root hairs from each specimen and then pre-treated each sample using the standard acid-base-acid (ABA) extraction method (Grootes et al., 2004) to isolate the humin fraction of the soil (thought to be the oldest, most nonreactive, and least contaminated organic component of the soil).

Sample $\delta^{13}C$ values range between –10.4 and –15.6, suggesting that isolated organic material derives from C4 plants. The ^{14}C results obtained at the National Ocean Sciences Accelerator Mass Spectrometry (NOSAMS) Facility give a variety of ages, and show a linear correlation between ^{14}C-age and $\delta^{13}C$, with older samples being enriched in ^{13}C. Kalapani Dam histosols are 1.79 ± 0.045, 23.5 ± 0.20, and 27.5 ± 0.18 ka; Kinhi Quarry histosols are 11.65 ± 0.07 and 13.15 ± 0.085 ka; and the pit histosol is 40.8 ± 1.1 ka.

It is not surprising that the histosols from different locations are different ages, as many generations of muddy wetland soils are visible even across the modern landscape. One interpretation of the data is that the very young 1.79 ka age represents modern contamination, the 11.65 ka measurement represents a maximum age for Lonar Crater, and the 23.5–40.8 ka ages are from older, pre-impact histosols. Such an interpretation would be broadly consistent with previous age estimates and the excellent state of preservation of Lonar Crater despite the seasonally wet monsoonal climate. To test this hypothesis, future work could attempt to isolate and date material such as pollen or charcoal that more clearly was deposited during histosol formation. Microscope work at the Limnological Research Center, University of Minnesota (Vania Stefanova and Amy Myrbo, 2005, personal commun.) did isolate Pinus and Tricolpate pollen, as well as charcoal, in our samples, but unfortunately not enough for material-specific AMS ^{14}C dating.

DISCUSSION

Preservation State and Reconstruction of Lonar Crater

Lonar Crater is a remarkably well-preserved impact crater. Ejecta preservation has been aided by light ground shrub cover (Fudali et al., 1980), and a reduction in surface runoff as a result of the high permeability of the ejecta blanket. The crater cavity and rim are protected by the state from new construction, but the ejecta blanket is not. Unfortunately for geologists, the residents of Lonar town and surrounding farms are steadily removing and reworking the ejecta blanket. Nevertheless there are rare areas where the presence of an impact spherule-rich layer suggests that the original ejecta surface of fine debris and impact glass has been unaltered by human activity or mass wasting.

The erosional state of Lonar is only a little more developed than that of Barringer Crater, which is similar in size and age to Lonar Crater. Roddy (1978) estimated from mass-balance considerations that erosion at Barringer Crater resulted in (1) a widening of the initial crater by 30 m to 1.186 km, and (2) a decrease in average rim height of 20 m, to a present-day value of 47 m. This erosion is equivalent to the removal of 20%–25% of the overturned flap and continuous ejecta blanket. Grant and Schultz (1993) estimated that erosion was less, with 10–15 m of rim height lowering and only one meter of removal of the continuous ejecta blanket. The rim-fold hinge at Barringer Crater is locally observed around a third of the crater rim (Shoemaker, 1963), compared to 10%–15% at Lonar.

Based on the mass of the sediments in the crater floor derived from five drill cores and a gravity survey, Fudali et al. (1980) estimated the original crater rim diameter to be 1710 m, for a widening of ~120 m. They also estimated an original rim height of 40 m, which was linearly extrapolated from the current outer rim crest slope to the original rim radius. Due to erosional shallowing of the original rim crest slope, this extrapolation must be considered a lower limit. Fudali et al. (1980) estimated the eroded volume of material deposited as sediments in the crater floor (modeled as a 1330 × 108 m cylinder) to be about 7×10^7 m^3 at the pre-impact density. Without further drilling or geophysical surveys of the crater floor and breccia lens, we have no means to improve upon this estimate of the eroded mass. We can revisit the original crater radius, by reconstructing an annulus of material along the crater wall. The height of the annulus is the sum of the present average lake to rim height of 135 m, the 108 m of sediments, and a few meters for the lake. The reconstructed radius is ~50 m smaller than the present radius, for an original rim diameter of 1780 m. The simple reconstruction is a rough estimate of the fresh crater diameter, as the contribution to the sediments from Dhar Canyon has not been separated from the average erosion around the crater wall.

Unfortunately, access to the breccia lens is severely limited by the crater lake and colluvium deposits. Knowledge about the breccia lens is primarily derived from five drill cores and a gravity survey (Fudali et al., 1980). At 400 m below the crater floor level, the cores did not conclusively penetrate through the breccia lens to the hard trap below, and there was no consistent correlation between the contents of each core. In an unpublished tomography survey conducted by India's National Geophysical Research Institute, the bottom of the breccia lens was constrained to be less than 500–750 m below the crater floor (S.S. Rai, 2005, personal commun.). More accurate measurements of the mass of the breccia lens would aid geometric reconstruction of the transient and final (pre-erosion) crater diameters.

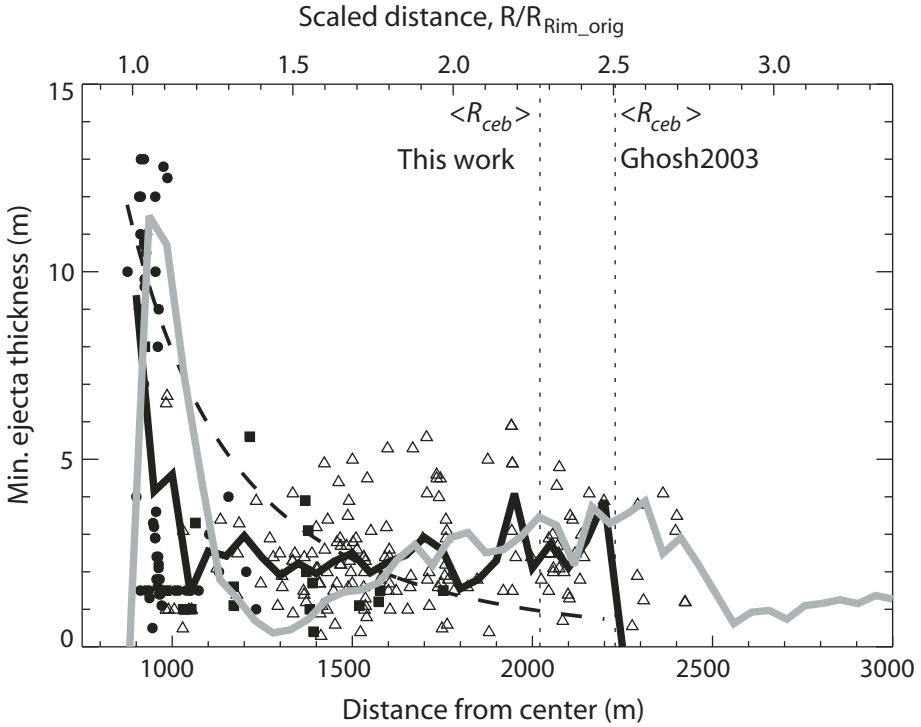

Figure 10. Minimum ejecta thickness measurements (filled circles—rim fold; filled squares—large blocks; open triangles—small clasts; see also Fig. 4) at Lonar Crater. Average Lonar ejecta thickness profile of the continuous ejecta blanket (solid black line, 50-m radial bins) is compared to a ballistic ejecta thickness from experimental craters (dashed line, McGetchin et al. [1973]) and the topographic profile for a typical fresh Martian crater (solid gray line, scaled to Earth, from Stewart and Valiant [2006]). R_{ceb} denotes the average extent of the continuous ejecta blanket (vertical dotted lines). Note accumulation of ejecta amounting to ~5 times ballistic predictions at the distal edge of continuous ejecta blanket.

Based on their (lower limit) reconstruction, Fudali et al. (1980) suggested that the rim height at Lonar was anomalously low. Typical rim heights around fresh simple craters are $0.036D_R$ for the Moon (Pike, 1977), $0.04D_R$ to $0.05D_R$ for Earth and Mars (Fudali et al., 1980; Stewart and Valiant, 2006), where D_R is the pre-erosion rim diameter. If Lonar were similar to other terrestrial craters with an original rim height of $0.04D_R$, the total thickness of the rim would be ~71 m (for D_R = 1780 m). Based on our DEM, the rim height above the pre-impact level varies from 18 m in the northeast (near Dhar Canyon) to 68 m in the southwest, which reflects the regional slope. We confirm that the average present-day rim height is ~30 m. In the rim-fold to the northwest and southeast, perpendicular to the regional slope, the total heights are 35 and 33 m, respectively. At these locations, the preserved ejecta deposit is ~10 m thick. A maximum average ejecta thickness of 13 m is observed on the north rim-fold (Fig. 4).

The extent of the uplifted strata in the rim-fold can be used to estimate the amount of erosion of the rim crest and the original rim height. The rim uplift constitutes 20%–40% of the total rim height in large experimental craters (Carlson and Jones, 1965; Dillon, 1972). Near the rim, the total thickness of ejecta and uplifted material decays with distance by a –3 power law (McGetchin et al., 1973). At the present-day rim radius of 940 m, the total thickness should be ~60 m. Hence, it is possible that ~30 m of rim crest topography has been removed and transported into the crater or outward into the near-rim ejecta blanket. Comparisons with the inferred amount of erosion for Barringer Crater indicate that this amount is a reasonable estimate. The stratigraphic uplift of ~20 m in the preserved rim-fold is ~33% of the expected original thickness (60 m), in perfect agreement with the range observed around experimental craters. Hence, the observed stratigraphic uplift suggests that the original rim height was typical of other terrestrial craters and implies an average of 30-m of vertical erosion at the present-day rim crest.

In summary, the estimated pre-impact rim diameter is 1780 m and rim height is ~70 m. The amount of observed uplifted strata at the rim is consistent with other simple impact and explosion craters.

Crater Wall Deformation

Because of the small size of the crater, rock and shock deformation features in the crater rim-fold and ejecta are limited. Microfaulting in the crater wall is difficult to observe because of the homogeneous nature of the target rock and preexisting jointing and flow banding. The strain from the rim-fold was primarily accommodated along contacts between Deccan flows. Although fracturing and brecciation clearly are pervasive in the overturned flap of the rim-fold, the tear zones do not penetrate as radial fractures with observable offset in the crater wall basalts below Tf5. In contrast, at Barringer Crater, tear faults are oriented parallel to an orthogonal set of preexisting regional vertical joints (Shoemaker, 1963; Kumar and Kring, 2008). In the absence of such large-scale preexisting weaknesses in the target, small crater dynamics may not result in large differential displacements in the crater wall (Melosh, 1989).

Because the rim-fold hinge is only locally preserved and landslide scars and rubble piles are abundant, normal faulting probably accommodated much of the post-impact crater wall collapse that generated some of the material that forms the breccia lens in the crater cavity. Although it is difficult to tell whether the normal faults at Fault Canyon continue to a depth below the crater lake, their dips must be shallow enough to cause 5°–10° of observed back rotation in the slump blocks. More often than not, the crater-rim–tangent normal faults themselves are not observed directly because the hanging-wall blocks have probably foundered into the lake. We cannot say for certain whether this normal faulting occurred immediately following crater formation, or subsequently over the past >~12,000 years.

Ejecta Volume

The good preservation of the ejecta allows us to estimate a total volume of the continuous ejecta blanket. Like at Barringer Crater, the amount of vertical erosion in the ejecta blanket is expected to be much less than at the rim crest, because the steep topography of the rim accelerates erosion compared to the gently sloping (2°–6°) ejecta blanket. A total ejecta volume estimate is constructed by binning all the minimum ejecta thickness measurements (Fig. 10) into 25–100 m increments in radial distance and calculating a solid of revolution assuming axisymmetry. We integrate the radial thickness profile between the present-day rim and a radial distance of 2200 m from center, which is the

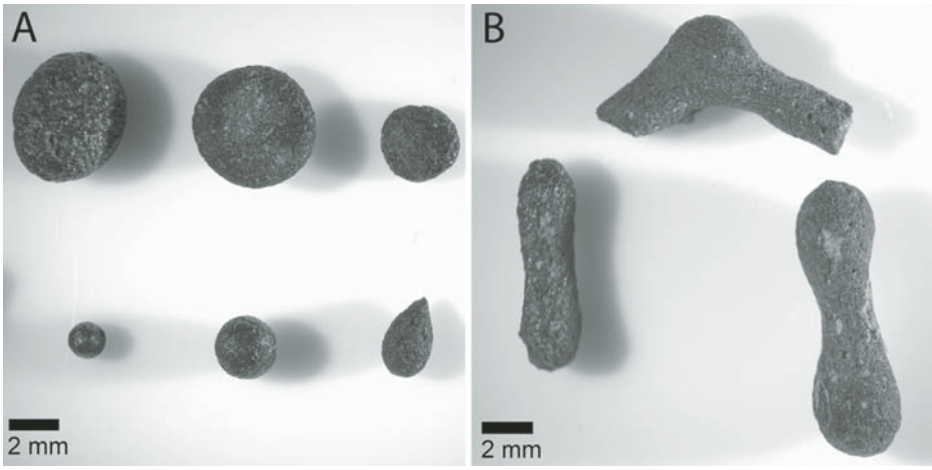

Figure 11. Basaltic impact glass spherules and flädle with a variety of splash forms recovered from undisturbed regions of the crater rim and at Little Lonar (Fig. 4). Note pancake-toroid (A—upper-middle) and dumbbell (B) forms.

average extent of the continuous ejecta blanket. Using the average value in each radial bin (solid black line in Fig. 10), the total ejecta volume is $3.4 \pm 0.3 \times 10^7$ m^3. Using the maximum value in each radial bin, the total ejecta volume is $6 \pm 1 \times 10^7$ m^3. The error denotes the 1σ sensitivity to bin size. We stress that the average ejecta volume should be considered a minimum value.

The excavated volume of material is difficult to predict because of uncertainties in the magnitude of widening between the transient and final crater diameters. Instead, we compare the Lonar ejecta volume to measured ejecta blanket volumes around Martian craters. Fits to measurements of continuous ejecta volumes around Martian craters with diameters of 3 km and larger predict ejecta volumes between $5 – 10 \times 10^7$ m^3 for Lonar-sized craters (Stewart and Valiant, 2006). An example measured Martian ejecta profile is shown in Figure 10 (solid gray line). The measured volume of ejecta around Martian craters was larger than could be explained by standard calculations of the excavated volume from the transient crater, even when accounting for reasonable amounts of bulking and addition of secondary materials. In order to fit the observed ejecta volumes, Stewart and Valiant (2006) needed to make a modification to the standard relationship between transient crater diameter at the preexisting surface level and final crater rim diameter. They found that the ratio should be ~1.4 (reduced from 1.56 recommended by Melosh [1989]). In other words, the amount of wall collapse in simple craters is reduced. The agreement between ejecta volumes around Lonar and Martian craters suggests that the same scaling modification applies to simple terrestrial craters.

The similarity between the volume of continuous ejecta deposits around Lonar Crater and fresh Martian impact craters also supports our inference of excellent preservation at Lonar Crater.

Ejecta Blanket Emplacement

The excellent exposure of the continuous ejecta blanket in multiple quarries makes Lonar an invaluable and unique site for study of ejecta emplacement processes. Assuming that the ejecta thickness profile at Lonar has not been altered significantly by erosion or human activities, the Lonar profile is remarkably similar to lobate, rampart-terminated ejecta blankets observed around fresh craters on Mars (solid gray line, Fig. 10). The profile consists of two sections: (1) an inner section that is composed primarily of large ejecta blocks that were not significantly mobilized post-emplacement, and (2) an outer ejecta section composed of smaller clasts and coarse matrix that was involved in a radial debris flow. In between the two sections is a moat-like feature in the ejecta profile that is commonly seen around Martian craters (Stewart and Valiant, 2006). Ramparts terminating Martian ejecta blankets are often scalloped or sinuous (Barlow, 1994) in a manner similar to Lonar Crater (Fig. 4).

The observed ejecta thickness profile significantly departs from the expected ballistic power law around small craters. In Figure 10, the –3 power law (dashed line) has the same volume as the average ejecta thickness profile (solid black line). In the outer ejecta (beyond 1400 m from crater center), the Lonar ejecta blanket has ~20%–30% more material compared to the power-law profile. The observations of lateral bulldozing, vertical mixing, and the lack of size sorting and stratification suggest that most of the outer continuous ejecta blanket was involved in a post-ballistic debris flow. The unsorted clasts and abrupt termination of the ejecta blanket imply a chaotic or turbulent ground-hugging debris flow, similar to the ejecta (Bunte Breccia) found at the larger Reis crater (Hörz et al., 1983). The amount of secondary materials mixed with the primary ballistic ejecta is not as significant as measured at Reis (up to >90% of the volume in the outer continuous ejecta) because most of the ballistic ejecta at Lonar impacted at velocities lower than, or comparable to, that needed for substantial secondary cratering (~100 m/s, Oberbeck, 1975). Hence, Lonar-sized craters may represent the transition between simple ballistic emplacement and ballistic sedimentation.

At Lonar, the shallow water table and surface mud deposits may have contributed to the ejecta dynamics; however, the ejecta deposit is not characteristic of clast size sorted water-supported debris flows on Earth. Estimates of the runout efficiency of ground-hugging ejecta flows on Mars are much less than found in terrestrial water-supported debris flows (Ivanov, 1996; Barnouin-Jha and Buczkowski, 2007). However, incorporation of groundwater may have fluidized the flows at Lonar (and Barringer) crater in ways still not fully understood.

Alternatively, shear in a weak basal layer has been suggested to support horizontal ejecta flow around larger craters on Earth and Mars. Modeling of Martian ejecta flows suggests that basal glide is the dominant flow mechanism (Barnouin-Jha et al., 2005). At Lonar, the muddy histosol may have contributed to basal glide. The flame structures (Figs. 9E and 9F) may have formed when basalt clasts in a ground-hugging debris surge impacted or bulldozed the underlying substrate. In most cases, the injected histosol was broken up by the ejecta flow into small clasts and incorporated into the matrix. (In order to preserve the observed histosol flame, the ejecta flow must have stopped just after its formation.) This observation is consistent with Fudali et al. (1980) who state that "final emplacement of most of the debris in the outer portions of the continuous blanket involved radial motion at very low angles, with enough force in the terminal stage to strongly affect the substrate." They cite examples of "large, individual blocks of ejecta ... [which] plowed along the original surface for some distance, bulldozing accumulations of soil ahead of them" in "some sort of ground-hugging debris surge." In other places (e.g., Kalapani Dam Quarry), the ejecta-histosol contact is a flat plane over several meters.

The departure from a monotonically decreasing thickness ejecta profile at Lonar Crater is

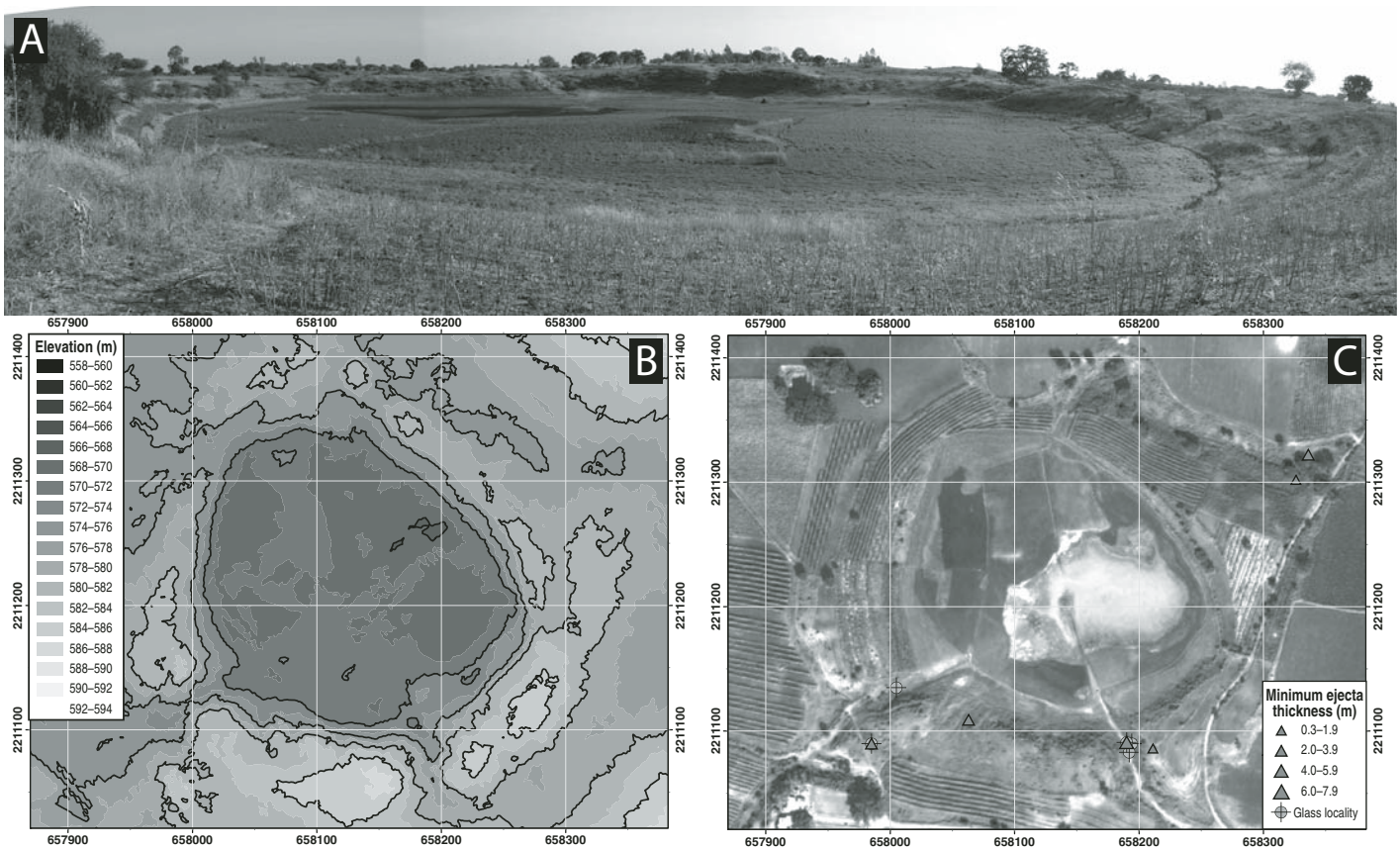

Figure 12. Panoramic photograph (A), digital elevation model (B; see Fig. DR12 [footnote 1]), and Quickbird satellite image (C) of Little Lonar, an ~300-m-diameter side depression located 700 m NNE of Lonar Crater (Fig. 1). Coordinates are Universal Transverse Mercator (UTM) (WGS84) in meters. Color version in GSA Data Repository [footnote 1].

not predicted by the ballistic sedimentation model. Distal thickening and rampart formation is expected for a debris flow with a friction-dominated ridge toe (Pierson and Costa, 1987; Major and Iverson, 1999). At this time, we are not able to accurately quantify the relative contributions from mixing of secondary materials and horizontal flow to the final ejecta profile; however, the low velocities (<150 m/s) associated with the ballistic ejecta and the abundant field evidence for horizontal flow suggest that the distal thickening of the continuous ejecta may be primarily a result of the post-ballistic, ground-hugging flow.

The atmospheres on Mars and Earth may have contributed to the flow dynamics. However, similar rampart ejecta structures have been observed around craters on the atmosphereless Jovian icy moon Ganymede (Boyce et al., 2008). Further work is necessary to understand the dynamics of the flow and the primary mechanism(s) that lead to the observed highly mobile behavior of ejecta around terrestrial and Martian craters.

CONCLUSIONS

We developed a digital elevation model and a geological map of Lonar Crater, India, with horizontal and vertical resolution of 1–3 m. Lonar Crater formed in at least six 10- to 25-m-thick basalt layers typical of inflated pahoehoe flows. The flows grade upward from massive fine-grained pipe-vesicle basalt to nonvesicular jointed and sometimes flow-banded basalt. Flow tops are often characterized by columnar jointing, and vesiculation and weathering.

Along the crater rim, the uppermost flow is recumbently (and parasitically) folded around rim concentric, subhorizontal, noncylindrical fold axes. Rim-folding was locally chaotic resulting in breccia blocks that have been shown to be randomly oriented through a paleomagnetic conglomerate test; the rim-fold hinge is preserved around only 10%–15% of the crater rim.

The present-day rim diameter is 1.88 ± 0.05 km. The erosional state of Lonar Crater is comparable to Barringer Crater, with an estimated decrease of the rim crest by ~30 m and an increase in the rim-to-rim crater radius of ~50 m. New radiocarbon dating of histosols and organic-rich swamp muds at the base of the ejecta blanket suggest a maximum age of ca. 12 ka for the impact event.

Unlike at Barringer Crater, no significant vertical displacement of the basalt flows in the crater walls was observed along identifiable tear zones. Layer-parallel slip between the two uppermost flows in the crater wall near Dhar Canyon was observed, consistent with slip along a weak contact during recumbent folding of the crater rim.

Millimeter- to centimeter-sized vesicular impact glasses were collected around the eastern and western rim of Lonar Crater. Many of these glasses are aerodynamically and rotationally sculpted and solidified during flight. Based on the stratigraphic distribution of impact glasses in the walls, an ~300 m depression known as Little Lonar, we conclude that the structure is not a second impact crater. The size, location, and stratigraphy of Little Lonar also rule out

secondary cratering as its origin. Rather, the depth of the depression has been exaggerated by clearing of its interior for farming and piling of material onto the surrounding wall.

The current continuous ejecta blanket has a scalloped distal termination. Occasionally, centimeter- to meter-sized blocks within the ejecta blanket locally penetrate the underlying histosol, deforming and mobilizing the histosol upward. More commonly, locally derived cm-sized rip-up clasts of histosol and similar sized ejecta clasts are incorporated in the debris flow and underlying histosol, respectively. Efficient turbulent mixing, a lack of sorting and stratification, and a distal overthickening of the ejecta blanket strongly support ejecta emplacement via a ground-hugging debris flow after the initial ballistic deposition.

The topographic profile of the continuous ejecta blanket, total volume, and distal structure are remarkably similar to fluidized ejecta features on Mars. Hence, Lonar Crater may be used to test different physical models for the formation of fluidized ejecta blankets.

ACKNOWLEDGMENTS

We thank Gordon Osinski, Senthil Kumar, and Christian Koeberl for thoughtful reviews. Maloof was supported by the Agouron Institute, and field research was funded by Harvard University and the National Aeronautics and Space Administration (NASA) Mars Fundamental Research Program (MFRP) grant NNG06GH34G. Julie Dickerson (Princeton '10) executed the illustrations accompanying field photographs, and Bill Guthe helped with geographic information system (GIS) computing. Preliminary petrographic and microprobe studies were performed by Evelyn Mervine (Massachusetts Institute of Technology and Woods Hole Oceanographic Institution). The authors benefited from discussions with Brad Samuels, Situ Studio, Peter Moore, Sue Trumbore, Horton Newsom, and Shawn Wright. We thank Jérôme Gattacceca for access to Le Centre Européen de Recherche et d'Enseignement des Géosciences de l'Environnement (CEREGE) facilities (Centre National de la Recherche Scientifique [CNRS], France). The field work would not have been as productive without translations, observations, and logistical support from Anand Misra, and excellent advice from Dhruba Mukhopadhyay. The Maharashtra Tourism Development Corporation (MTDC) hotel at Lonar kept us healthy and happy.

REFERENCES CITED

Ahrens, T.J., Xia, K., and Coker, D., 2002, Depth of cracking beneath impact craters: New constraint for impact velocity, *in* Furnish, M.D., Thadhani, N.N., and Horie, Y., eds., Shock Compression of Condensed Matter–2001: Melville, New York, American Institute of Physics, p. 1393–1396.

Ai, H.A., and Ahrens, T.J., 2006, Simulation of dynamic response of granite: A numerical approach of shock-induced damage beneath impact craters: International Journal of Impact Engineering, v. 33, p. 1–10, doi: 10.1016/j.ijimpeng.2006.09.046.

Barlow, N., Stewart, S., and Barnouin-Jha, O., 2005, The role of volatiles and atmospheres on Martian impact craters: Eos (Transactions, American Geophysical Union), v. 86, p. 433, doi: 10.1029/2005Eo440009.

Barlow, N.G., 1994, Sinuosity of Martian rampart ejecta deposits: Journal of Geophysical Research, v. 99, p. 10,927–10,935, doi: 10.1029/94JE00636.

Barlow, N.G., 2005, A review of Martian impact crater ejecta structures and their implications for target properties, *in* Kenkmann, T., Horz, F., and Deutsch, A., eds., Large meteorite impacts III: Geological Society of America, p. 433–442.

Barlow, N.G., and Bradley, T., 1990, Martian impact craters: Correlations of the ejecta and interior morphologies with diameter, attitude, and terrain: Icarus, v. 87, p. 156–179, doi: 10.1016/0019-1035(90)90026-6.

Barlow, N.G., Boyce, J.M., Costard, F.M., Craddock, R.A., Garvin, J.B., Sakimoto, S.E.H., Kuzmin, R.O., Roddy, D.J., and Soderblom, L.A., 2000, Standardizing the nomenclature of Martian impact crater ejecta morphologies: Journal of Geophysical Research, v. 105, p. 26,733–26,738, doi: 10.1029/2000JE001258.

Barnouin-Jha, O.S., and Buczkowski, D.L., 2007, Comparing the runout of fluidized ejecta on Mars with mass movements on Earth: 38th Lunar and Planetary Science Conference: Houston, Texas, Lunar and Planetary Institute, Abstract no. 1304.

Barnouin-Jha, O.S., and Schultz, P., 1998, Lobateness of impact ejecta deposits from atmospheric interactions: Journal of Geophysical Research, v. 103, p. 25,739–25,756, doi:10.1016/S0734-743X(99)00061-5.

Barnouin-Jha, O.S., and Schultz, P., 1999, Interactions between an impact generated ejecta curtain and an atmosphere: International Journal of Impact Engineering, v. 23, p. 51–62, doi: 10.1016/S0734-743X(99)00061-5.

Barnouin-Jha, O.S., Baloga, S., and Glaze, L., 2005, Comparing landslides to fluidized crater ejecta on Mars: Journal of Geophysical Research, v. 110, p. E04010, doi: 10.1029/2003JE002214.

Beals, C., Innes, M., and Rottenberg, J., 1960, The search for fossil meteorite craters: Current Science, v. 29, p. 205–245.

Blanford, W., 1870, Notes on route from Poona to Nagpur, vid Ahmednuggur, Jalna, Loonar, Yeotmahal, Mangali and Hingunghat: Records of the Geological Survey of India, v. 1, p. 60–65.

Bondre, N., Duraiswami, R., and Dole, G., 2004, Morphology and emplacement of flows from the Deccan Volcanic Province, India: Bulletin of Volcanology, v. 66, p. 29–45, doi: 10.1007/s00445-003-0294-x.

Boyce, J.M., Nadine, N.R., Mouginis-Mark, P.J., and Stewart, S.T., 2008, Rampart craters on Ganymede: Their implications for fluidized ejecta emplacement: Meteoritics and Planetary Science.

Brandt, D., and Reimold, W., 1995, The geology of the Pretoria Saltpan Impact structure and the surrounding area: South African Journal of Geology, v. 98, p. 287–303.

Carlson, R.H., and Jones, G.D., 1965, Distributions of ejecta from cratering explosions in soils: Journal of Geophysical Research, v. 70, p. 1897–1910, doi: 10.1029/JZ070i008p01897.

Carr, M., Crumpler, L., Cutts, J., Greeley, R., Guest, J., and Masursky, H., 1977, Martian impact craters and emplacement of the ejecta by surface flow: Journal of Geophysical Research, v. 82, p. 4055–4065, doi: 10.1029/JS082i028p04055.

Chakrabarti, R., and Basu, A.R., 2006, Trace element and isotopic evidence for Archean basement in the Lonar crater impact breccia, Deccan Volcanic Province: Earth and Planetary Science Letters, v. 247, p. 197–211, doi: 10.1016/j.epsl.2006.05.003.

Chenet, A., Quidelleur, X., Fluteau, F., Courtillot, V., and Bajpal, S., 2007, ^{40}K-^{40}Ar dating of the Main Deccan large igneous province: Further evidence of KTB age and short duration: Earth and Planetary Science Letters, v. 263, p. 1–15, doi: 10.1016/j.epsl.2007.07.011.

Cisowski, S., 1975, The effect of shock on the magnetic moments and hysteresis properties of natural materials, with special emphasis on rocks from the Lonar meteorite crater, India, and their relationship to lunar paleomagnetism: Meteoritics, v. 10, p. 383.

Cotton, C., 1944, Volcanoes as landscape forms: Christchurch, New Zealand, Whitcombe and Tombs Limited, 416 p.

Crawford, A., 1983, Mantle convection pattern under India: Relevance to Lonar Crater, Girnar Node and peri-Indian volcanism: Journal of the Geological Society of India, v. 24, p. 97–100.

Cressie, N., 1993, Statistics for spatial data, revised edition: New York, John Wiley and Sons, 900 p.

Deshmukh, S., 1988, Petrographic variations in compound flows of Deccan traps and their significance, *in* Subbarao, K., ed., Deccan flood basalts: Memoirs of the Geological Society of India, v. 10, p. 305–319.

Dillon, L., 1972, The influence of soil and rock properties on the dimensions of explosion-produced craters: Kirtland Air Force Base, New Mexico, Technical Report AFWL-TR-71-144, Air Force Weapons Laboratory, p. 171.

Dube, A., and Sengupta, S., 1984, Detailed investigation of Lonar crater, Buldana Distrct, Maharashtra: Unpublished Report, Geological Survey of India, field seasons 1971–1972 to 1978–1979, Geological Survey of India, referenced by Ghosh and Bhaduri (2003).

Duraiswami, R., Dole, G., and Bondre, N., 2003, Slabby pahoehoe from the western Deccan Volcanic Province: Evidence for incipient pahoehoe-aa transitions: Journal of Volcanology and Geothermal Research, v. 121, p. 195–217, doi: 10.1016/S0377-0273(02)00411-0.

Fredriksson, K., Dube, A., Milton, D., and Balasundaram, M., 1973a, Lonar Lake, India: An impact crater in basalt: Science, v. 180, p. 862–864, doi: 10.1126/science.180.4088.862.

Fredriksson, K., Noonan, A., and Nelen, J., 1973b, Meteoritic, lunar and Lonar impact chondrules: The Moon, v. 7, p. 475–482, doi: 10.1007/BF00564647.

Fredriksson, K., Brenner, P., Dube, A., Milton, D., Mooring, C., and Nelen, J., 1979, Petrology, mineralogy, and distribution of Lonar (India) and lunar impact breccias and glasses: Smithsonian Contributions to the Earth Sciences, v. 22, p. 1–12.

Fudali, R., and Fredriksson, K., 1992, Tektite-like bodies at Lonar Crater, India—Very unlikely: Meteoritics, v. 27, p. 99–100.

Fudali, R.F., Milton, D.J., Fredriksson, K., and Dube, A., 1980, Morphology of Lonar Crater, India: Comparisons and implications: The Moon and the Planets, v. 23, p. 493–515, doi: 10.1007/BF00897591.

Ghosh, S., 1996, Studies on the possible size, shape and nature of impactite in Lonar Crater, Buldana District, Maharashtra: Unpublished Report, Geological Survey of India, Field Season 1993–1994, Geological Survey of India, referenced by Ghosh and Bhadur (2003).

Ghosh, S., 2003, Is Lonar astrobleme an example of cometary impact?: Indian Minerals, v. 57, p. 105–114.

Ghosh, S., and Bhadur, S., 2003, Petrography and petrochemistry of impact melts from Lonar Crater, Buldana Distract, Maharashtra, India: Indian Minerals, v. 57, p. 1–26.

Gilbert, G., 1896, The origin of hypotheses, illustrated by the discussion of a topographic problem: Science, v. 3, p. 1–13, doi: 10.1126/science.3.53.1.

Grant, J.A., and Schultz, P.H., 1993, Degradation of selected terrestrial and Martian impact craters: Journal of Geophysical Research, v. 98, p. 11,025–11,042, doi: 10.1029/93JE00121.

Grieve, R.A.F., Garvin, J.B., Coderre, J.M., and Rupert, J., 1989, Test of a geometric model for the modification stage of simple impact crater development: Meteoritics, v. 24, p. 83–88.

Grootes, P., Nadeau, M., and Rieck, A., 2004, ^{14}C-AMS at the Leibniz-Labor: Radiometric dating and isotope research: Nuclear Instruments and Methods in Physics Research, Section B, Beam Interactions with Materials and Atoms, v. 223–224, p. 55–61, doi: 10.1016/j.nimb.2004.04.015.

Herrick, R., and Pierazzo, E., 2003, Improving knowledge of impact cratering: Bringing together "modelers" and "observationalists": Eos (Transactions, American Geophysical Union), v. 84, p. 291, doi: 10.1029/2003EO310006.

Hörz, F., 1965, Untersuchungen an Riesgläsern: Beiträge zur Mineralogie und Petrographie, v. 11, p. 621–661, doi: 10.1007/BF01128707.

Hörz, F., Ostertag, R., and Rainey, D.A., 1983, Bunte breccia of the Ries: Continuous deposits of large impact craters: Reviews of Geophysics and Space Physics, v. 21, p. 1667–1725, doi: 10.1029/RG021i008p01667.

Ivanov, B.A., 1996, Spread of ejecta from impact craters and the possibility of estimating the volatile content of the Martian crust: Solar System Research, v. 30, p. 36–50.

Jagla, E.A., and Rojo, A.G., 2002, Sequential fragmentation: The origin of columnar quasihexagon patterns: Physical Review E: Statistical, Nonlinear, and Soft Matter Physics, v. 65, p. 026203, doi: 10.1103/PhysRevE.65.026203.

Jhingran, A.G., and Rao, K.V., 1958, Lonar Lake and its salinity: Records of the Geological Survey of India, v. 85, p. 313–334.

Kenkmann, T., 2002, Folding within seconds: Geology, v. 30, p. 231–234, doi: 10.1130/0091-7613(2002)030<0231:FWS>2.0.CO;2.

Kenkmann, T., and Ivanov, B.A., 2006, Target delamination by spallation and ejecta dragging: An example from the Ries crater's periphery: Earth and Planetary Science Letters, v. 252, p. 15–29, doi: 10.1016/j.epsl.2006.08.024.

Kenkmann, T., and Schonian, F., 2006, Ries and Chicxulub: Impact craters on Earth provide insights for Martian ejecta blankets: Meteoritics and Planetary Science, v. 41, p. 1587–1603.

Kieffer, S.W., and Simonds, C.H., 1980, The role of volatiles and lithology in the impact cratering process: Reviews of Geophysics and Space Physics, v. 18, p. 143–181, doi: 10.1029/RG018i001p00143.

Kieffer, S.W., Schaal, R.B., Gibbons, R., Hoerz, F., Milton, D.J., and Dube, A., 1976, Shocked basalt from Lonar impact crater, India, and experimental analogues, *in* Proceedings, 7th Lunar Science Conference: New York, Pergamon Press, p. 1391–1412.

Kring, D., 1995, The dimensions of the Chicxulub impact crater and impact melt sheet: Journal of Geophysical Research, v. 100, p. 16,979–16,986, doi: 10.1029/95JE01768.

Kuiper, K., Deino, A., Hilgen, F., Krijgsman, W., Renne, P., and Wijbrans, J., 2008, Synchronizing rock clocks of Earth history: Science, v. 320, p. 500–504, doi: 10.1126/science.1154339.

Kumar, P.S., 2005, Structural effects of meteorite impact on basalts: Evidence from Lonar Crater, India: Journal of Geophysical Research, v. 110, p. B12,402, doi:10.1029/2005JB003662.

Kumar, P.S., and Kring, D.A., 2008, Impact fracturing and structural modification of sedimentary rocks at Meteor Crater, Arizona: Journal of Geophysical Research, v. 113, doi: 10.1029/2008JE003115.

Lafond, E.C., and Dietz, R.S., 1964, The Lonar Crater (India)-meteorite crater: Journal of the Indian Geophysical Union, v. 1, p. 91–97.

LaTouche, T., 1912, The geology of Lonar Lake: Records of the Geological Survey of India, v. 41, p. 266–275.

Louzada, K.L., Weiss, B.P., Maloof, A.C., Stewart, S.T., Swanson-Hysell, N.L., and Soule, S.A., 2008, Paleomagnetism of Lonar impact crater, India: Earth and Planetary Science Letters, v. 275, p. 308–319, doi: 10.1016/j.epsl.2008.08.025.

Major, J., and Iverson, R., 1999, Debris-flow deposition: Effects of pore-fluid pressure and friction concentrated at flow margins: Geological Society of America Bulletin, v. 111, p. 1424–1434, doi: 10.1130/0016-7606(1999)111<1424:DFDEOP>2.3.CO;2.

Malcolmson, J., 1840, On the fossils of the eastern portion of the great basaltic district of India: The Geological Society of London, v. 5, p. 537–575.

Master, S., 1999, Evidence for an impact origin of the Ambar Lake structure: A smaller companion crater to the Lonar impact crater, Maharashtra, India: Johannesburg, South Africa, 62nd Meteoritical Society Meeting, Lunar and Planetary Institute, Abstract no. 5086.

McElhinny, M., 1964, Statistical significance of the fold test in palaeomagnetism: Geophysical Journal International, v. 8, p. 338–340.

McGetchin, T. R., Settle, M., and Head, J.W., 1973, Radial thickness variation in impact crater ejecta: Implications for lunar basin deposits: Earth and Planetary Science Letters, v. 20, p. 226–236, doi:10.1016/0012-821X(73)90162-3.

Melosh, H.J., 1989, Impact cratering: New York, Oxford University Press, 245 p.

Melosh, H.J., and Beyer, R., 1998, Crater program: http://www.lpl.arizona.edu/tekton/crater.html.

Melosh, H.J., and Ivanov, B.A., 1999, Impact crater collapse: Annual Review of Earth and Planetary Sciences, v. 27, p. 385–415, doi: 10.1146/annurev.earth.27.1.385.

Mishra, S.P., 1987, Lonar Lake and co-linear carbonatites of Western India: Journal of the Geological Society of India, v. 29, p. 344–348.

Morgan, J.W., 1978, Lonar Crater glasses and high-magnesium australites: Trace element volatilization and meteoritic contamination, *in* Proceedings, 9th Lunar and Planetary Science Conference: New York, Pergamon Press, v. 2, p. 2713–2730.

Morrison, R., and Oberbeck, V., 1978, A composition and thickness model for lunar impact crater and basin deposits, *in* Proceedings, 9th Lunar and Planetary Science Conference: New York, Pergamon Press, p. 3763–3785.

Mouginis-Mark, P.J., 1978, Morphology of Martian rampart craters: Nature, v. 272, p. 691–694, doi: 10.1038/272691a0.

Murali, A.V., Zolensky, M.E., and Blanchard, D.P., 1987, Tektite-like bodies at Lonar Crater, India—Very unlikely. Comment on: Tektite-like bodies at Lonar Crater, India: Implications for the origin of tektites, *in* Proceedings, 17th Lunar and Planetary Science Conference, Part 2: Journal of Geophysical Research, v. 92, no. B4, p. E729–E735, doi: 10.1029/JB092iB04p0E729.

Nandy, N., and Deo, V., 1961, Origin of Lonar Lake and its salinity: TISCoP, v. 8, p. 1–2, referenced by Ghosh and Bhaduri (2003).

Nayak, V.K., 1972, Glassy objects (impactite glasses?): A possible new evidence for meteoritic origin of the Lonar Crater, Maharashtra State, India: Earth and Planetary Science Letters, v. 14, p. 1–6, doi:10.1016/0012-821X(72)90070-2.

Nayak, V.K., 1993, Maskelynite from the Indian impact crater at Lonar: Journal of the Geological Society of India, v. 41, p. 307–312.

Newsom, H.E., Nelson, M.J., Shearer, C.K., and Draper, D., 2005, Hydrothermal alteration at Lonar Crater, India and elemental variations in impact crater clays: Houston Texas, 36th Lunar and Planetary Science Conference, Lunar and Planetary Institute, Abstract no. 1143.

Oberbeck, V., 1975, The role of ballistic erosion and sedimentation in lunar stratigraphy: Reviews of Geophysics and Space Physics, v. 13, p. 337–362.

Orlebar, A., 1839, Account of the Lake Lonar: Transactions of the Bombay Geographical Society, v. 1, p. 9–43.

Osae, S., Misra, S., Koeberl, C., Sengupta, D., and Ghosh, S., 2005, Target rocks, impact glasses and melt rocks from the Lonar impact crater, India: Petrography and geochemistry: Meteoritics and Planetary Science, v. 40, p. 1473–1492.

Osinski, G., Grieve, R., and Spray, J., 2004, The nature of the groundmass of surficial suevites from the Ries impact structure, Germany, and constraints on its origin: Meteoritics and Planetary Science, v. 39, p. 1655–1684.

Pierson, T., and Costa, J., 1987, A rheologic classification of subaerial sediment-water flows: Geological Society of America Reviews in Engineering Geology, v. 7, p. 1–12.

Pike, R.J., 1976, Crater dimensions from Apollo data and supplemental sources: The Moon, v. 15, p. 463–477, doi: 10.1007/BF00562253.

Pike, R.J., 1977, Size-dependence in the shape of fresh impact craters on the Moon, *in* Roddy, D.J., Pepin, R.O., and Merrill, R.B., eds., Impact and explosion cratering: New York, Pergamon Press, p. 489–509.

Polanskey, C.A., and Ahrens, T.J., 1990, Impact spallation experiments: Fracture patterns and spall velocities: Icarus, v. 87, p. 140–155, doi: 10.1016/0019-1035(90)90025-5.

Poornachandra Rao, G., and Bhalla, M., 1984, Lonar lake: Palaeomagnetic evidence of shock origin: Geophysical Journal of the Royal Astronomical Society, v. 77, p. 847–862.

Roddy, D.J., 1978, Pre-impact conditions and cratering processes at Meteor Crater, Arizona, a typical bowl-shaped crater, *in* Proceedings, 9th Lunar and Planetary Science Conference: Houston, Texas, Pergamon Press, v. 2, p. 3891–3930.

Roddy, D.J., Pepin, R.O., and Merrill, R.P., 1977, Impact and explosion cratering: New York, Pergamon Press, 1302 p.

Schaal, R.B., 1975, Shock metamorphism in basalt from Lonar Crater, India and in six lunar microcraters [M.Sc. thesis]: Los Angeles, University of California, 143 p.

Schultz, P., 1992, Atmospheric effects on ejecta emplacement: Journal of Geophysical Research, v. 97, p. 11,623–11,662, doi: 10.1029/92JB00889.

Sengupta, D., and Bhandari, N., 1988, Formation age of the Lonar Crater: Houston, Texas, 19th Lunar and Planetary Science Conference, Lunar and Planetary Institute, p. 1059–1060.

Sengupta, D., Bhandari, N., and Watanabe, S., 1997, Formation age of Lonar Meteor Crater, India: Revista de Fisica Aplicada e Instrumentacao, v. 12, p. 1–7.

Shoemaker, E., 1960, Penetration mechanics of high velocity meteorites, illustrated by Meteor Crater, Arizona, *in* 21st International Geological Congress: Copenhagen, Report, pt. 18, p. 418–434.

Shoemaker, E.M., 1963, Impact mechanics at Meteor crater, Arizona, *in* Kuiper, G., and Middlehurst, B., eds., The Moon, meteorites and comets: Chicago, Illinois, University of Chicago Press, p. 301–336.

Son, T.H., and Koeberl, C., 2007, Chemical variation in Lonar impact glasses and impactites: GFF, The Geological Society of Sweden, v. 129, p. 161–176.

Stewart, S.T., and Valiant, G.J., 2006, Martian subsurface properties and crater formation processes inferred from fresh impact crater geometries: Meteoritics and Planetary Science, v. 41, p. 1509–1537.

Stewart, S.T., Ahrens, T.J., and O'Keefe, J.D., 2004, Impact processing and redistribution of near-surface water ice on Mars, *in* Furnish, M.D., Gupta, Y.M., and Forbes, J.W., eds., Shock Compression of Condensed Matter–2003: Melville, New York, American Institute of Physics, p. 1484–1487.

Storzer, D., and Koeberl, C., 2004, Age of the Lonar Impact Crater, India: First results from fission track dating: Houston, Texas, 35th Lunar and Planetary Science Conference, Lunar and Planetary Institute, Abstract no. 1309.

Subrahmanyam, B., 1985, Lonar Crater, India: A cryptovolcanic origin: Journal of the Geological Society of India, v. 26, p. 326–335.

Taiwade, V., 1995, A study of Lonar lake—A meteorite-impact crater in basalt rock: Bulletin of the Astronomical Society of India, v. 23, p. 105–111.

Vandamme, D., Courtillot, V., Besse, J., and Montigny, R., 1991, Paleomagnetism and age determinations of the Deccan traps (India): Results of a Nagpur-Bombay traverse and review of earlier work: Reviews of Geophysics, v. 29, p. 159–190, doi: 10.1029/91RG00218.

Weiss, B., Garrick-Bethell, I., Pedersen, S., Maloof, A., Louzada, K., and Stewart-Mukhopadhyay, S., 2007, Paleomagnetism of impact glass and spherules from Lonar Crater, India: Houston, Texas, 38th Lunar and Planetary Science Conference, Lunar and Planetary Institute, Abstract no. 2360.

Wittmann, A., Kenkmann, T., Hecht, L., and Stoffler, D., 2007, Reconstruction of the Chicxulub ejecta plume from its deposits in drill core Yaxcopoil-1: Geological Society of America Bulletin, v. 119, p. 1151–1167, doi: 10.1130/B26116.1.

Manuscript Received 3 June 2008
Revised Manuscript Received 8 November 2008
Manuscript Accepted 15 November 2008

Printed in the USA